

Nomenclature

PID Controller = Proportional Integral Derivative Controller

PD Controller = Proportional Derivative Controller

IMU = Inertial Measurement Unit

IC = Internal Combustion

F = Frequency

V = Voltage

ω_f = Fan Speed (RPM)

RPM = Revolutions per minute

RPS = Revolutions per second

N = Number of fan blades

P = Power (W)

I = Current (A)

T = Thrust

t = time (s)

CFD = Computational Fluid Dynamics

g = Acceleration due to gravity

F_D = Drag Force

ρ_{air} = Density of air

A = Area

v = *velocity*

T_S = Settling time

ζ = damping ratio

ω_n = Natural frequency

D(s) = Disturbance Force

h = height of platform above ground level

b_1 = constant relating to the frictional force experienced by the platform for vertical motion

b_2 = constant relating to the drag force experienced by the platform for vertical motion

T_1 = thrust produced by the central fan

T_2, T_3, T_4, T_5 = Thrust produced by each of the four perimeter fans respectively

1. Introduction

1.1 Project Aim & Individual Tasks

The project aim was to design and develop a fully autonomous flying platform, the product design specifications of which have been included in section 1.2. To achieve this goal each group member was tasked to work on certain aspects of the design and hence had individual project aims. The main individual aims achieved and outlined in this report are as follows:

- Determination of relevant system parameters from the testing of the perimeter fans.
- The development of an accurate mathematical model of the flying platform.
- The design and development of the stability control system.
- The design and development of the height control system.

1.2 Product Design Specification (PDS)

The PDS for this year's group project can be found in Appendix A, Table A1. The following design requirements and improvements in addition to those specified last year are as follows:

- Onboard Power in the form of an internal combustion engine must be incorporated. The IC engine should supply direct mechanical drive to the larger central fan, and hybrid electrical power to the perimeter fans.
- The incorporation of a higher quality sensor in the form of an IMU which will give simultaneous control of pitch, roll, and height must also be adopted.

Whilst achieving these points the following further developments were kept in mind to allow next year's project group to continue with minimal modification to the power and control systems:

- Extending control to allow for yaw
- Controlling horizontal flight

2. Background Research

2.1 Previous Flying Platform Project 2003

The structure of the flying platform project 2003 consisted of a basic five ducted fan platform, fabricated predominantly from aluminium alloy [1]. The height and stability control were effectively split into two separate sections. The perimeter fans were used to control the platform stability of the platform whilst the central fan was used to control the height. An analogue PID controller was developed to control the stability of the system, while a PD controller was designed to control the height. The control values were all set as variables and hence could be adjusted with potentiometers to refine the control system during testing.

On testing the stability control in one axis, the control system maintained stability for over 2 minutes. However the platform was not tested in dual axis flight, and hence it could not be ascertained if stability could be maintained with increased degrees of freedom. The findings from the previous group's project were encouraging and hence a similar system was hoped to be implemented using the same five fan design with the perimeter fans controlling the system stability, and the central fan controlling the height.

The main concern from last year's analysis was the stability control only being maintained for a few minutes before the system would lose control. On further analysis of Stephen Moore's report [2] many fundamental errors were found within the design of the stability control system, with even the basic mathematical model containing errors. On discussing this with Mustafa Aziz, Exeter University lecturer, it materialised the majority of the stability control had been determined through an iterative trial and error process through experimenting with the platform. It was speculated that this is perhaps why the stability control was only capable of stabilisation for a few minutes. Another contributing factor to the stability only being controlled only for a few minutes was that the platform structure was designed in such a manner to make the platform inherently unstable. See Chapter 4 for further details on this issue. It is consequently hoped that in altering the structural design, the stability control performance will be significantly enhanced.

3. Testing of Control Fans

3.1 Introduction

Due to the implementation of an IC engine in this year's project, an accurate understanding of the power requirements of the platform was needed, before an appropriate IC engine could be selected and purchased. To achieve this and to be able to calculate other system requirements, tests were run on the control fans to determine the following:

- The relationship between the thrust produced and the power required.
- The relationship between the inputted pulse width signal and the corresponding thrust produced.
- The relationship between the inputted pulse width signal and the corresponding fan speed generated.
- The peak power requirements of the control fans.
- The response time of the fans and hence the transfer function for the fan motors.
- Whether the control fans would overheat during operation.
- The point where ground effects become negligible.

To determine these factors, 5 experiments were carried out and have been explained in the sections to follow. Prior to carrying out these experiments a means of measuring the fan speed was required and is covered in the next section.

3.2 Fan Speed Measurement

To measure the rotational fan speed accurately a laser pen was set up in a manner to project a beam of light through the duct and onto a photo transistor positioned on the opposite side of the fan (see Figure 1 overleaf). As the fan rotated the laser beam was broken and a 5V pulse generated by the photo transistor. These pulses were then inputted into a frequency to voltage converter. This would produce a voltage that would directly correspond to the frequency and consequently allow the fan speed to be determined.

As the maximum safe operating speed of the perimeter fan is 35,000 RPM [3], it was decided the method used would not have to measure speeds exceeding this value. Due to the fan having 6 blades this would require frequencies of up to 3500 Hz to be measured. This resulted in a frequency to voltage converter being constructed whose circuit diagram can be seen in Appendix B, Figure B1.

On testing the circuitry with a square wave input with amplitude 5V from a signal generator, a plot of voltage against frequency was created (see Figure B2), and a linear relationship found. This relationship yielded Equation 1, which enables a direct conversion from the voltage output, to the frequency.

$$F = 666.67 \cdot V \quad \text{Equation 1}$$

To convert the frequency into a fan speed in terms of RPM Equation 2 can be used.

$$\omega_f = \frac{60 \cdot F}{n} \quad \text{Equation 2}$$

Combining Equations 1 & 2 yields a direct relation between the voltage output from the frequency to voltage converter, and the fan speed in terms of RPM as follows:

$$\omega_f = 6666.7 \cdot V \quad \text{Equation 3}$$

On testing the circuitry with the fan, the blades did not break the laser beam for an adequate period of time to generate a square wave form from the photo transistor. This led to the addition of an operational amplifier in the circuitry shown in Figure B1. This made the pulses swing high and low between +5V and 0V. Consequently a much squarer signal was produced and inputted into the frequency to voltage converter, allowing the fan speed to be successfully measured.

3.3 General Test Method

To carry out testing on the perimeter fans the apparatus was set up as shown in Figure 1 overleaf. The laser pen was held in position with a clamp stand, and the photo transistor was fixed to the table top with masking tape. The counterbalance was then adjusted so a small load would be registered on the scales. The scales were then zeroed. It should be noted that the position of the pivot is not equidistant between the scales and the fan; hence the principle of moments must be used to convert the mass reading from the scales into a thrust produced by the fan.

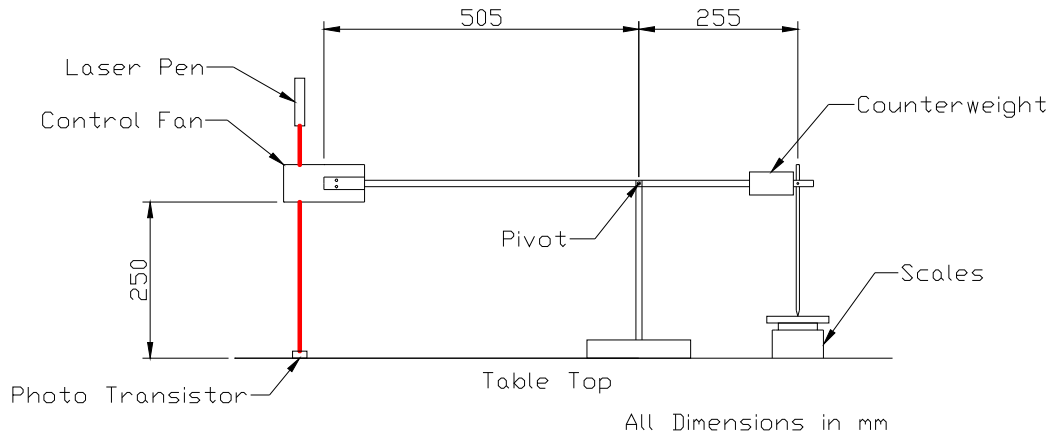


Figure 1: Set up of apparatus

Pulse width modulation was used to control the fan speed. This works by varying the duty of a square wave input to the fan's speed controller, which in turn generates the required fan speed. Alex Tombling created some software to produce the required pulse width modulated signals (for further information refer to Alex Tombling's individual report [4]). The stop signal was set to a pulse width of 1 ms (5% duty) and the full speed signal was set to a 2ms pulse width (10% duty). Anything in between represented a percentage of the top speed.

Two lead acid batteries were used to power the fan. A multi-meter and an ammeter were connected to the batteries to determine the current and voltage drawn by the fan motor. A multi-meter was also connected to a thermister situated by the fan motor in order to monitor the motor temperature. With the test apparatus fully set up and checked the experiments covered in the sections to follow were carried out.

3.4 Experiment 1: Thrust & Power Testing

3.4.1 Method

With the apparatus and equipment set up as stated in section 3.3, testing could begin. The software was programmed to increment the pulse width by 0.05 ms. This would effectively allow the fan speed to be changed by 5% increments of the top speed. The fan was then started up and run at 7% of the maximum speed. The mass on the scales, and the voltage and current drawn from the battery were then recorded. The voltage produced from the frequency to voltage converter was also recorded and the temperature of the fan motor was continually monitored in the event of overheating occurring.

The fan speed was then increased to 10% of the maximum power and the respective mass, voltage and current readings were recorded. The fan speed from this point on was then incremented by 5% of the maximum speed and the appropriate readings recorded until the top speed of the fan was reached. This experiment was then repeated two further times, to limit the possibility of errors creeping into the results.

3.4.2 Results

The mean reading for each appropriate fan speed was tabulated and can be seen in Appendix C, Table C1. From the mean readings recorded the fan speed was calculated using Equation 3. The thrust was then also calculated using the principle of moments. These results have also been recorded in Table C1. Various plots were then created to observe different characteristics of the perimeter fan.

The first graph, Figure C1, confirms a linear relationship to exist between the fan speed and the input pulse width signal, provided the fan is operating within 10-90% of the maximum fan speed. The non-linear region existing below 10% and above 90% of the fan's top speed means to enable an accurate comparison over the entire speed range, all further test parameters should be compared to the RPM measured and not the input signal.

Figure C2 shows the relationship between the thrust and the fan speed. Unfortunately there is no distinct linear region within which the fans could be made to operate. This will make the control of the stability of the platform a little more complex. However, a clear quadratic relationship does exist, and a trend line has been added to the graph including the equation of the trend line. This relationship will be required later in determining the transfer function for the control fans.

The final graphs produced were to determine the optimal point where the greatest amount of thrust could be generated for the least amount of increase in power. Figure C3 shows a plot of the input power against thrust produced, however from this plot it is a little difficult to determine the optimal point, consequently Figure C4 was created. Figure C4 shows a plot of the Thrust/Power against the fan speed. From this the optimum point can be clearly seen to occur at a fan speed of 7000 RPM which produces a corresponding thrust of 0.92 N with an input power requirement of 25.1 W.

3.4.3 Conclusions

Although the optimum amount of lift with regard to input power was determined to be at a point where 0.92 N of thrust would be generated, this will not be the chosen operating point. This is due to the estimated overall lift requirements being substantially higher than this value. It has been estimated that the control fans will have to produce a minimum of 9.9 N (1 kg) of thrust. This will require an input power of 410 W per perimeter fan which unfortunately is at the lower end of the thrust per power efficiency curve.

Operating the control fans to generate 9.9 N of thrust will require the fans to be run at 60% of the fan's top speed. This is well within the linear region observed for the input pulse width signal against the fan speed produced, and will make control of the fans simpler. It should be noted that later on in the project, once circuitry had been designed and built by Alex Tombling to generate the pulse width signals, a test of the circuitry produced a completely linear relationship throughout the entire speed range. This indicated that perhaps the PC had produced a faulty signal below a pulse width of 1.1 ms and above 1.9 ms, producing the non linear results observed in testing.

3.5 Experiment 2: Peak Power Requirements

3.5.1 Method

This experiment was carried out to determine the peak power requirements of the perimeter fans. To achieve this, an estimation was made that in a worst case scenario the fans would have to make a control correction resulting in a sudden 3 N (300 g) increase of thrust. This would relate to a 10% increase in fan speed. Consequently the fan was set to run at the previously determined 60% of top speed, and then underwent a sudden increase to 70% of the top speed. A multi-meter and ammeter had already been set up to record the maximum voltage and current drawn from the battery during this sudden increase in thrust. This was repeated 3 times and the mean voltage and current calculated. Equation 4, given below, was then used to determine the peak power required.

$$P = I \cdot V$$

Equation 4

3.5.2 Results

The results from experiment 2 have been recorded in Table 1 below.

Table 1: Results from experiment 2

Change in Fan Speed	Peak Current (A)	Peak Voltage (V)	Peak Power (W)
60% - 70%	30.2	24.2	731
60% - 70%	30.2	24.1	728
60% - 70%	29.5	24.1	711
Mean Reading	30	24.1	723

The fans running at 60% require a power input of 410 W, hence an increase of up to 313 W may be required for a sudden stability control correction. This must be allowed for when determining the generation set requirements.

3.6. Experiment 3: Determination of the Fan Response Times

3.6.1 Method

To determine the response times of the perimeter fans the voltage output from the frequency to voltage converter was connected to an oscilloscope. The output from the PC producing the required pulse width signal was also connected to the same oscilloscope. This allowed the oscilloscope to be triggered by a change in pulse width from the PC, enabling the voltage output from the frequency to voltage converter to be recorded.

This set up allowed an accurate recording of the fan speed to be taken against time, allowing exactly when the fan speed had reached its steady state output to be determined. The true response time of the fans should be determined by when the thrust reached its steady state value, however it would have been impractical for an individual to read the scales over a 0.3 second timescale at 0.01 s intervals. Consequently the quadratic relationship determined in section 3.4.2 from the graph in

Figure C2 was used to convert the fan speed into a corresponding thrust. This meant an assumption was made that the thrust corresponding to the fan speed would be generated instantly. In reality there would be a small lag time between the change in fan speed generating the equivocal change in thrust, however as this lag time would be minimal, it can be neglected and hence our assumption will be valid. The response times for a 5% and 10% increment in pulse width were then measured using this method. Again as with previous experiments the method was repeated and the mean readings determined.

3.6.2 Results

The response times corresponding to the appropriate changes in pulse width can be found in Appendix D, Table D1. The tabulated data representing the change in fan speed, and hence thrust with time can be seen in Table D2. A graph representing this data is shown in Figure D1. A trend line was added to the graph including the equation of the line. This equation is shown below in Equation 5.

$$T = 69.167 \cdot t^3 - 53.994 \cdot t^2 + 14.291 \cdot t + 14.632 \quad \text{Equation 5}$$

3.6.3 Conclusions

Testing revealed the response times of the fans to be adequate enough to maintain the stability of the platform. The cubic relationship observed between the thrust and time can later be used to determine the transfer function for the control fans. This will be explained in chapter 5.5.

3.7 Experiment 4: Monitoring of Fan Temperature

3.7.1 Method

To ascertain whether the fans were prone to overheating under prolonged operation the following experiment was carried out. A thermister was situated next to the fan motor and connected to a multi-meter to enable a temperature reading to be taken. The motor specification sheet [3], stated the motor should not exceed temperatures of 100°C. The fan was then set to run at 60% of the top fan speed, and a stop watch was started to enable recordings of the temperature to be taken every 20 s.

The fan was kept running until the temperature stabilised. Once the temperature had stabilised the fan was set to idle at 10% of the top speed to allow the motor to cool at an increased rate. The final stage was then to shut down the fan completely and continue to monitor the temperature until it was decided that the motor had sufficiently cooled and there would be no further risk involved.

3.7.2 Results

The results for each of the three stages of the experiment have been tabulated and can be found in Appendix E, Tables E1 to E3. Three graphs were created of temperature against time for stages 1 to 3 and can be found in Figures E1 to E3 respectively. Figure E1 shows the motor temperature to stabilise at 63°C after approximately 600 s of operation. During stage 2 the fan temperature suddenly increased to 75°C before rapidly cooling to 43°C at which point the fan was shut down. At this point a sharp increase in temperature to 48°C was observed before the fan gradually began to cool.

3.7.3 Conclusions

The testing confirmed the fans could sustain prolonged periods of operation without overheating. However, the substantial increases in temperature noted on turning the fan off, has led to the following shut down procedure being specified. After fan use, the fans must be set to idle at 10% of the top fan speed for 6 minutes. This will allow adequate cooling of the fan to prevent overheating.

3.8 Experiment 5: Determination of the Extent of Ground Effects

3.8.1 Method

Ground effects will increase the amount of thrust produced by the fan when the fan is within a certain distance from the ground. This could produce problems with the height control during take off and landing. For this reason it must be determined at what height ground effects become negligible and if possible design the platform in a manner so the fans can be kept above this height. It was decided that if ground effects were found to be negligible at a height of 0.25 m, then this would be sufficient as the platform design could incorporate a landing stand allowing the fans to be a minimum distance of 0.25m from the ground.

As the initial thrust test results in experiment 1 had been carried out at a height of 0.25 m it was decided to re-run these test with the fan at a height of 1.17 m above the ground. These results could then be compared with those in experiment 1. If the results were the same then ground effects could be assumed to be negligible at heights above 0.25 m.

3.8.2 Results

The test results have been tabulated and can be seen in Appendix F, Table F1. A graph of the thrust test results at a height of 1.17 m and 0.25 m was then created and can be seen in Figure F1. The graph shows the results to be very similar. Thus ground effects can be assumed to be negligible for heights above 0.25 m.

3.8.3 Conclusions

As the test results have concluded ground effects to be negligible above heights of 0.25 m, a design constraint has been created in that the control fans must be situated a minimum 0.25 m above the ground.

4. Structure

4.1 Structure Stability

4.1.1 Theory

With any flying object there are two key points which determine its stability. These points are the centre of lift and the centre of mass. Whatever the orientation of the object these two points will remain in the same positions. It is the position of these two points with respect to one another that will determine whether an object will be inherently stable or not. For example when the centre of mass is below the centre of lift and a small angular displacement occurs, a self righting moment is produced, and the body is said to be in stable equilibrium (see Figure 2). If on the other hand the centre of mass is above the centre of lift and a small angular displacement occurs an overturning moment will be produced and the body is said to be in an unstable equilibrium (see Figure 3).

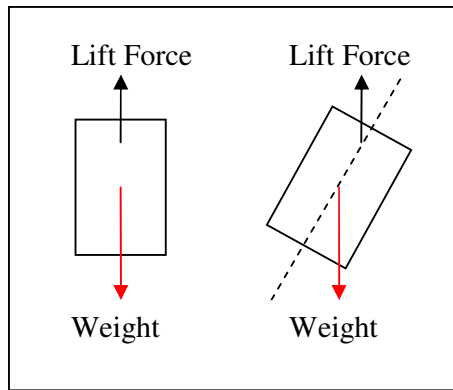


Figure 2: Stable Equilibrium

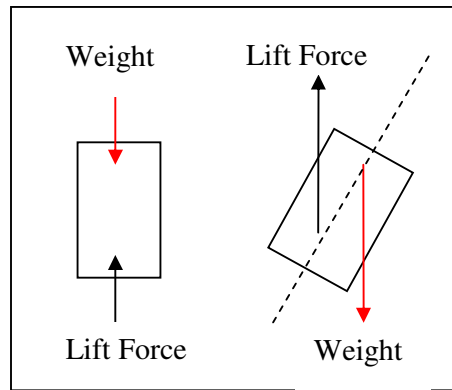


Figure 3: Unstable Equilibrium

4.1.2 Conclusions

For the platform stability control to be significantly improved the platform must be designed in a manner to allow the structure to be inherently stable. Another factor to be considered when designing the platform in this manner is the periodic time of oscillation. This shall be covered in section 4.2

4.2 Periodic Time of Oscillation

4.2.1 Theory

The periodic time of oscillation is dependent on the distance between the centre of mass and the centre of lift. This distance will form another important design constraint, as the periodic time of oscillation must be slower than the response time of the fans by a factor of 4. If it is not, the complexity of the control problem will be increased as the controllers will have to compensate for the time difference by increasing the rise time.

To determine a relationship between the periodic time of oscillation and the distance between the centre of mass to the centre of lift, a simple pendulum model representing the platform was created, and can be seen in Figure 4 overleaf.

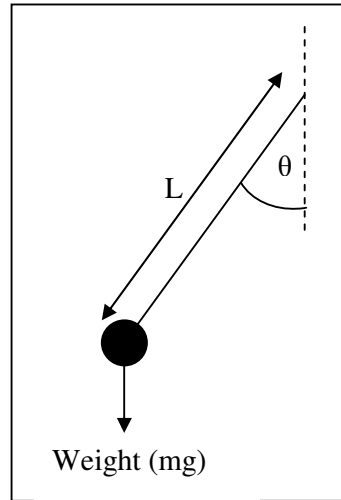


Figure 4: Pendulum model of the platform

Resolving the forces perpendicular to the pendulum arm gives:

$$F = m \cdot g \cdot \sin \theta \quad \text{Equation 6}$$

However for small angles: $\sin \theta \approx \theta$ so:

$$F = m \cdot g \cdot \theta \quad \text{Equation 7}$$

Newton's second law states that when a force is applied to a body the force produces an acceleration. The acceleration is directly proportional to the force, with the constant of proportionality being the mass of the body. This relationship can be used in conjunction with Equation 7 to form Equation 8 as follows:

$$-m \cdot g \cdot \theta = m \cdot L \cdot \frac{d^2 \theta}{dt^2} \quad \text{Equation 8}$$

Rearranging Equation 8 gives:

$$\frac{d^2 \theta}{dt^2} + \frac{g \cdot \theta}{L} = 0 \quad \text{Equation 9}$$

From the equations for simple harmonic motion it can be stated that:

$$\theta = A \cdot \cos \omega \cdot t + B \sin \omega \cdot t \quad \text{Equation 10}$$

Where: A = a constant

B = a constant

ω = the frequency

Differentiating Equation 10 with respect to time then gives:

$$\frac{d\theta}{dt} = -A \cdot \omega \sin \omega \cdot t + B \cdot \omega \sin \omega \cdot t \quad \text{Equation 11}$$

When $t = 0$ we know that $\left. \frac{d\theta}{dt} \right|_{t=0} = B \cdot \omega$, and the boundary conditions are such that

when $t = 0$, $\frac{d\theta}{dt} = 0$, therefore $B = 0$. Substituting this in to Equation 11 then gives:

$$\frac{d\theta}{dt} = -A \cdot \omega \sin \omega \cdot t \quad \text{Equation 12}$$

Also substituting B = 0 into Equation 10 gives:

$$\theta = A \cos \omega \cdot t \quad \text{Equation 13}$$

Taking Equation 12 and differentiating with respect to t will then yield:

$$\frac{d^2\theta}{dt^2} = -A \cdot \omega^2 \cos \omega \cdot t \quad \text{Equation 14}$$

Substituting Equations 14 and 13 into Equation 9 then gives:

$$-A \cdot \omega^2 \cos \omega \cdot t + \frac{g}{L} \cdot A \cos \omega \cdot t = 0 \quad \text{Equation 15}$$

This can be simplified to give:

$$\omega = \sqrt{\frac{g}{L}} \quad \text{Equation 16}$$

The equation for the periodic time in terms of the frequency is given in Equation 16 below.

$$T = \frac{2 \cdot \pi}{\omega} \quad \text{Equation 17}$$

Substituting Equation 16 into Equation 17 then gives:

$$T = 2 \cdot \pi \sqrt{\frac{L}{g}} \quad \text{Equation 18}$$

Equation 18 is the final relationship between the periodic time and the distance, L, between the centre of lift and mass. To understand this relationship a little more clearly a plot has been created of the periodic time against the distance between the centres of masses, L, and is shown below in Figure 5.

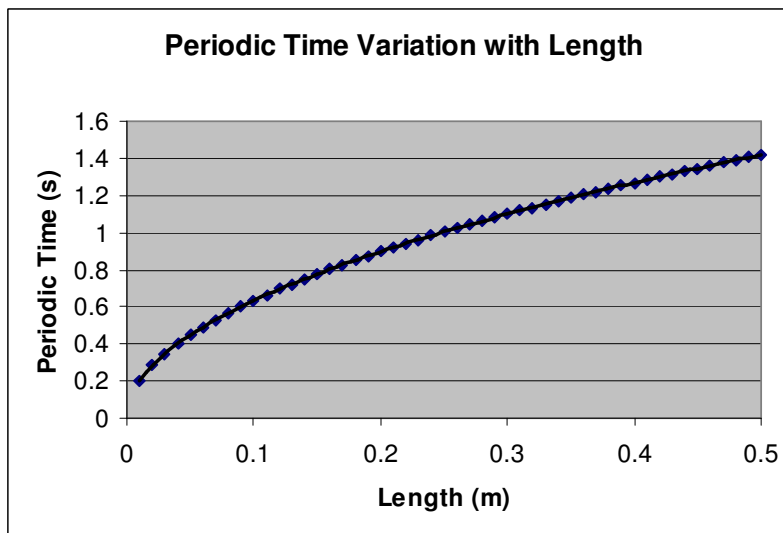


Figure 5: Graph of the periodic time of oscillation against the distance between the centre of mass and lift

4.2.2 Conclusions

In order for the platform to be controlled the response time of the fans must be faster than one quarter of the periodic time. For the worst case scenario previously determined, the response time of the fan was 0.3 s, substituting four times this value into Equation 18 for the periodic time gives the minimum possible value for L as 35.8 cm. If the platform design can not incorporate such a large value for L, then the controllers will have to compensate for this, by increasing the rise time of the response. This is not such a favourable solution however it is a perfectly plausible one.

4.3 Flow divergence of central & control fans

4.3.1 Introduction

As the previous constraints determined for the structure implicated a lower platform beneath the fans would be required, a concern was raised as to how the lower platform would distort the airflow from the fans. This distortion would inevitably reduce the amount of thrust generated. Hence it was decided a CFD simulation should be run in order to determine how much the airflow diverges on leaving the duct. This information could then be used to design a lower platform that would provide minimal distortion to the airflow.

4.3.1 Geometry and Flow Specifications

The geometry for the simulations has been specified in mm in Figure 6. The dimensions used to simulate the duct were taken from the central fan. During testing carried out by Richard Holbrook the velocity of the air speed expelled from the duct was measured at 30 m/s. This value was thought to be an underestimation of the actual air speed expelled during operation, however the slower the air speed the more the air flow will diverge, so running a simulation with an inlet velocity set to this value should provide a worst case scenario. The other boundary conditions set were the duct sides as walls, with all other edges defined as pressure outlets.

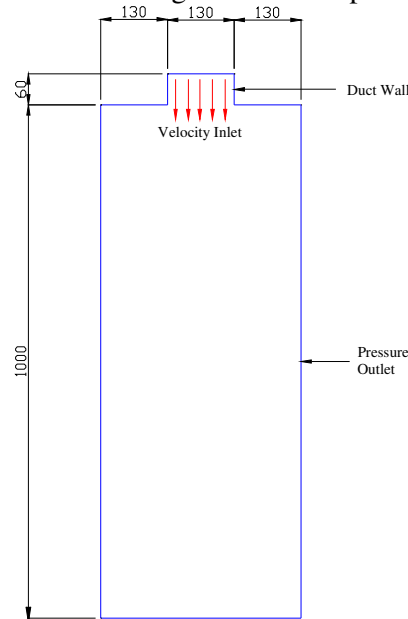


Figure 6: The simulation geometry and boundary conditions

4.3.2 Mesh Convergence

When carrying out CFD simulations the mesh refinement plays an important role in the accuracy of the solution. Generally the finer the mesh is the greater the accuracy of the solution, however increasing the number of mesh elements increases the amount of computational time required. This means a balance must be struck between the two factors. The process carried out to determine this balance point is known as mesh convergence.

To determine whether a mesh has been adequately refined, a preliminary coarse mesh is constructed and a simulation run and a specific factor observed, in this case the velocity in the y direction across the outlet at a 1 m distance downstream of the duct was used. The mesh was then refined by a factor of 2 and the simulation repeated. The velocity in the y direction across the outlet 1 m downstream of the duct was then observed and compared to the results obtained from the coarser mesh. If the results obtained were the same then the coarse mesh will be adequate to run all further simulations with, however if the results are different then further mesh refinement will be required.

Initially an interval size along the length of the geometry was set at 20 mm, with an interval size around the perimeter of the duct being 5 mm. The interval size across the outlet was also set to 5 mm. The mesh was then refined by a factor of 2. Figure 7 shows a graph comparing the results from both meshes. As the results are very similar it can be safely concluded that the initial mesh constructed was already adequately refined. The initial coarse mesh was then used for all further simulations.

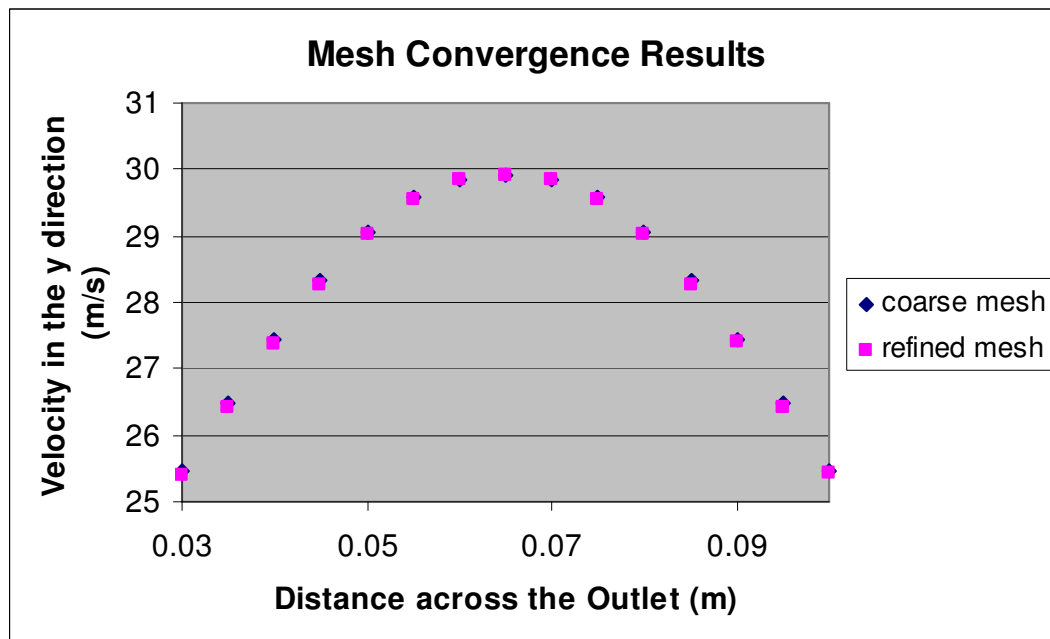


Figure 7: Graph showing mesh convergence has been achieved

4.3.3 Results

On running the simulation in Fluent using the standard k-ε model a contour plot of the velocity profile was created and can be seen in Figure 8. The contour plot shows clearly how the stream of air created by the ducted fan diverges outwards with increasing distance from the duct.

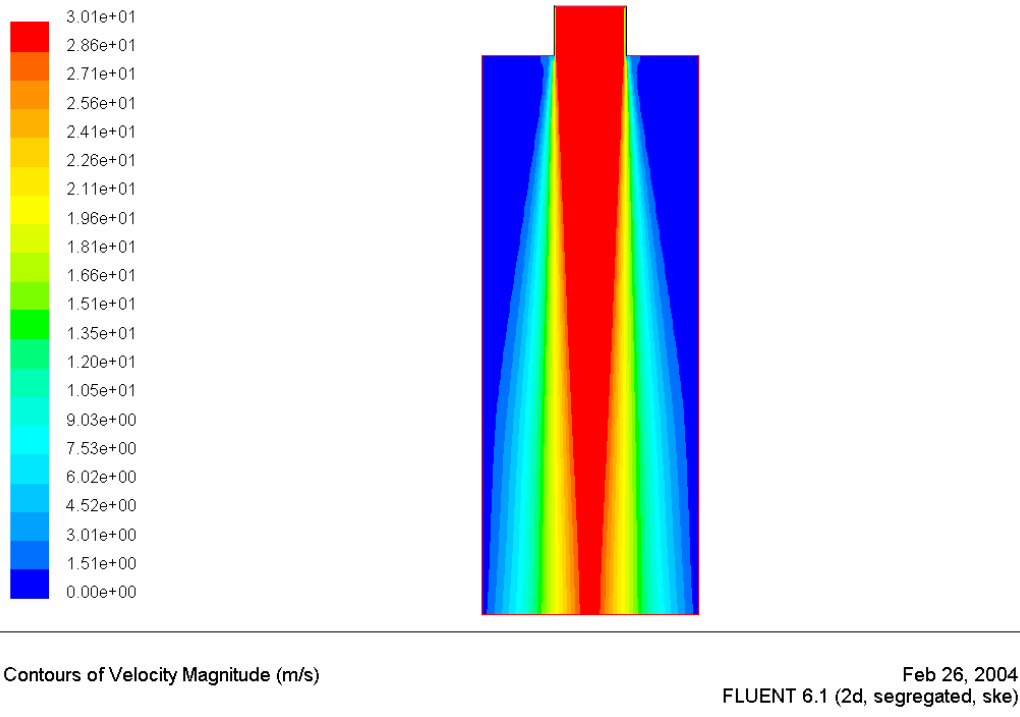


Figure 8: Contour plot of velocity

To determine accurately the degree to which the flow diverges, plots were created of the velocity in the y direction across the width of the stream at 500 mm and 1000 mm downstream of the duct. These plots can be seen in Appendix G, Figures G1 & G2. Figure G1 shows the results when an inlet velocity of 30 m/s was specified and Figure G2 shows the results when an inlet velocity of 100 m/s was specified. Comparing the two graphs also confirms the assumption that the slower the velocity of air expelled from the duct the more the air flow will diverge as a consequence.

4.3.4 Conclusions

From the results shown in Figure G1 it can be safely concluded that the flow will diverge by no more than 150 mm either side of the duct wall up to a distance of 1000mm downstream of the duct. Consequently when considering the design of the lower platform structure a safe distance of 300mm should be added to the diameter of the ducts. This should allow for a large enough circular hole for the airflow to bypass the lower mounting platform through.

Assuming last years dimensions are adopted with the control fans being placed a distance of 500mm from the central fan, a ring would have to be constructed for the lower platform with the dimensions shown in Figure 9.

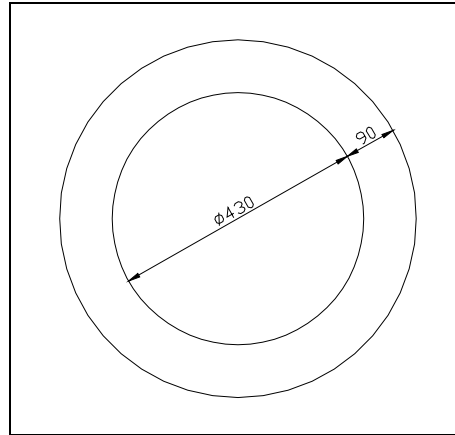


Figure 9: Dimension constraints for the lower platform

From these dimensions one can see that the width of the ring may not be thick enough to mount certain components on; consequently to increase the width of the ring will mean an increase in the distance between the perimeter fans if obstruction of the airflow is to be avoided. This should pose no problems when considering the control aspects, however an increase in the total mass of the flying platform will inevitably be incurred and with tight weight restrictions this may pose a problem. Another possible solution would be to increase the length of the duct, thus inhibiting the amount of divergence that would occur. This method however, would also add weight to the platform. To ascertain the best design for optimising the thrust to weight ratio, further in depth analysis will have to be carried out.

5. Stability Control

5.1 Mathematical Model

To construct an accurate mathematical model of the system in one axis a simple model of the system with the centre of mass lying directly beneath the centre of lift was considered and has been shown in Figure 10.

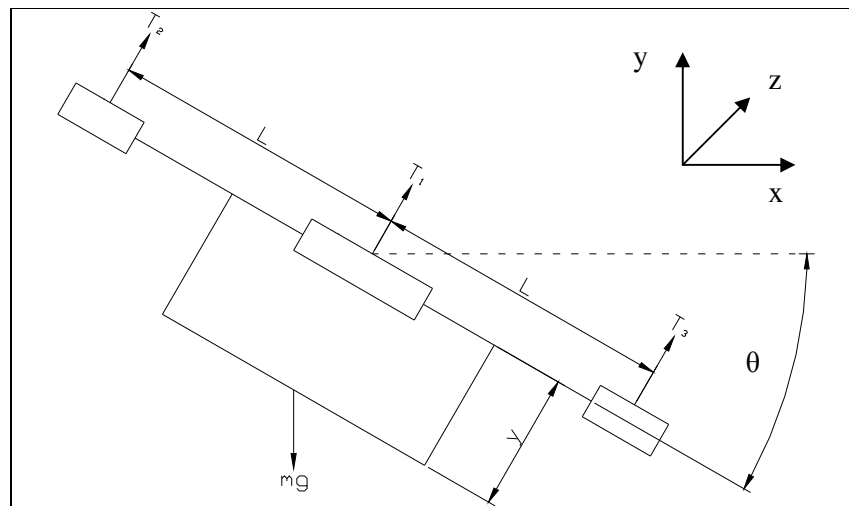


Figure 10: 2D diagram of the flying platform in one axis

From this model the total moments acting on the system can be determined, and have been expressed in Equation 19. Equation 19 has been fully derived in Appendix H, section 1.

$$M = T_2 \cdot L - T_3 \cdot L - m \cdot g \cdot y \sin \theta - m \cdot \omega^2 \cdot y^2 \sin \theta \cdot \cos \theta - k_2 \cdot \left(\frac{d\theta}{dt} \right)^2 - k_1 \cdot \frac{d\theta}{dt}$$

- Equation 19

Where: M = Total moments acting on the system.

T_2 = Thrust from control fan indicated in Figure 10 as T_2 .

T_3 = Thrust from control fan indicated in Figure 10 as T_3 .

L = Distance from the central fan to the control fan indicated in Figure 10.

m = Total mass of the platform.

g = Acceleration due to gravity.

y = distance of the centre of mass from the centre of lift indicated in Figure 10.

θ = Angular displacement.

ω = Rotational velocity in the x-z plane as defined in Figure 10, also referred to as the rate of gyroscopic precession.

k_1 = a constant representing the frictional force.

k_2 = a constant representing the drag force.

Newton's second law for a rotating body has been stated in Equation 20.

$$M = I \cdot \frac{d^2\theta}{dt^2}$$

Equation 20

Where: I = Total moment of inertia of the structure.

Equation 19 can then be substituted into Equation 20 to give the non linear model of the platform shown in Equation 21.

$$\frac{d^2\theta}{dt^2} = \frac{1}{I} \left(T_2 \cdot L - T_3 \cdot L - m \cdot g \cdot y \sin \theta - m \cdot \omega^2 \cdot y^2 \sin \theta \cdot \cos \theta - k_1 \cdot \frac{d\theta}{dt} - k_2 \cdot \left(\frac{d\theta}{dt} \right)^2 \right)$$

- Equation 21

5.2. Linearisation of the Mathematical Model

In order to design a controller for any non linear system, an approximated linear mathematical model must be used. This will enable design methods such as frequency response to be used in determining an effective system controller. The most common method used to achieve this is linearisation about an equilibrium point. Equation 22 represents the general equation used to linearise a non linear equation about the equilibrium point, θ_s . The equilibrium point in this case is when the platform is horizontal i.e. when $\theta = 0$.

$$f(\theta_s + \delta\theta) = f(\theta_s) + \left. \frac{df}{d\theta} \right|_{\theta=\theta_s} \cdot \delta\theta$$

Equation 22

Appendix H, section 2, shows how Equation 21 has been linearised to give Equation 23.

$$T_2 \cdot L - T_3 \cdot L = I \cdot \ddot{\theta} + k_1 \cdot \dot{\theta} + m \cdot g \cdot y \cdot \theta + m \cdot \omega^2 \cdot y^2 \cdot \theta \quad \text{Equation 23}$$

After carrying out linearisation on Equation 21 an intriguing point to note occurred.

The drag force term, $k_2 \left(\frac{d\theta}{dt} \right)^2$, disappeared where as the frictional force term, $k_1 \cdot \frac{d\theta}{dt}$, remained. This is a little concerning as the frictional force should be relatively minimal in comparison to the drag force. This will mean the linear model of the platform will give an underestimation of the total damping experienced by the system. For this reason it was decided that Equation 21 should be solved numerically in MathCAD and later compared to the transfer function results for a step input. This would allow the accuracy of the linearised solution to be validated against the non linear solution.

Before carrying out any numerical simulations, the design parameters must be defined. As the platform had not been fully designed and built, this proved a little tricky, and meant some estimations had to be made based on last years platform and the current design constraints. The design parameters have been specified in Table 2 below. The parameters taken from this years design were taken from Christopher Poczka's Report [5] and have been referenced within Table 2.

Table 2: Design parameters

Mass [5]	8.17 kg
Length of platform arm, L [5]	0.5 m
Distance between the centre of mass and the centre of lift, y [5]	0.2 m
Moment of Inertia	1.05 m ⁴
Rotational velocity of the platform, ω	0.3 rad s ⁻¹
Coefficient of moment due to Friction, k_1	0.5
Coefficient of moment due to drag, k_2	0.01875
Density of air, ρ_{air}	1.2 kg m ⁻³
Effective cross sectional area of the platform, A	1 m ²

The value of k_1 has been adopted from last years project [6] however this should be experimentally determined once the structure has been built. This can be done by suspending the platform at the point where the centre of lift is located, and applying a step force to start the platform oscillating. The frequency at which the platform is oscillating can then be measured. The damping ratio can then also be determined by measuring the settling time, T_s , and substituting these values into Equation 24. The settling time represented in Equation 24 is defined as the time taken for the system output to settle within 2% of the input amplitude.

$$T_s = \frac{4}{\zeta \cdot \omega_n} \quad \text{Equation 24}$$

A general form of a second order transfer function in terms of the natural frequency, damping ratio, and gain parameter, expressed in Equation 25, can then be equated to Equation 23. This will then allow k_1 to be determined in terms of the experimentally measured natural frequency and damping ratio. This has been expressed in Equation 26.

$$\ddot{y}(t) + 2 \cdot \zeta \cdot \omega_n \cdot \dot{y}(t) + \omega_n^2 \cdot y(t) = k \cdot \omega_n^2 \cdot u(t) \quad \text{Equation 25}$$

Where: k = the system's gain parameter

$$k_1 = 2 \cdot \zeta \cdot \omega_n \quad \text{Equation 26}$$

Unfortunately the structure was not constructed in time to allow the experimentally determined value of k_1 to be included within this report. Consequently the value for k_1 has been taken from last year's project, and has a value of 0.5.

k_2 was calculated by assuming the platform to behave as a large square panel (1 m² in area) rotating through the air. This allowed the drag force to be determined as follows:

$$F_D = \rho_{air} \cdot A \cdot v^2 \quad \text{Equation 27}$$

However the velocity varies with the distance, r , from the centre of the square panel by the following relationship:

$$v = r \cdot \frac{d\theta}{dt} \quad \text{Equation 28}$$

Substituting this into Equation 27 will then give the drag force; however this must be converted into a moment and hence must be multiplied by, r , to give the moment due to drag, M_D .

$$M_D = \rho_{air} \cdot A \cdot \left(\frac{d\theta}{dt} \right)^2 \int_0^L r^3 dr \quad \text{Equation 29}$$

This then becomes:

$$M_D = \rho_{air} \cdot A \cdot \left(\frac{d\theta}{dt} \right)^2 \cdot \frac{L^4}{4} \quad \text{Equation 30}$$

Substituting the appropriate values from Table 2 into Equation 30 then yields:

$$M_D = 1.2 \times 1 \times \frac{0.5^4}{4} \times \left(\frac{d\theta}{dt} \right)^2 \Rightarrow 0.01875 \cdot \left(\frac{d\theta}{dt} \right)^2 \quad \text{Equation 31}$$

Equating equation 31 to the term expressing the moment due to drag, $k_2 \left(\frac{d\theta}{dt} \right)^2$, gives the value of $k_2 = 0.01875$. These values can now be used to solve the non linear equation numerically and to determine the transfer function for the platform.

5.3 Transfer Function

The platform transfer function is simply formed by taking the Laplace transform of Equation 23. This yields the following equation:

$$T(s) = \left(\frac{1}{L} \right) (I \cdot s^2 \cdot \Theta(s) + k_1 \cdot s \cdot \Theta(s) + m \cdot y(g + \omega^2 \cdot y)\Theta(s)) \quad \text{Equation 32}$$

Rearranging Equation 32 then gives the transfer function for the platform in general terms as follows:

$$\frac{\Theta(s)}{T(s)} = \frac{L}{I \cdot s^2 + k_1 \cdot s + m \cdot y(g + \omega^2 \cdot y)} \quad \text{Equation 33}$$

A consideration that has not yet been looked into is the gyroscopic precession of the platform. This has been thus far represented by ω and assumed to be a constant. However in reality this value will fluctuate, the maximum value of which can not be ascertained until experimental flight has been carried out. For this reason it has been decided to look at the sensitivity of the system to changes in the magnitude of ω , and hence ascertain as to whether this would cause substantial problems in the stability control.

To determine the sensitivity of the system to ω , will require a comparison to be drawn between the magnitude of the $\omega^2 \cdot y$ term with respect to g . Assuming a value for $\omega = 0.3 \text{ rad s}^{-1}$, will give a magnitude of $\omega^2 \cdot y = 0.018$, this as a percentage of g (9.81 m s^{-2}) represents 0.18%. Even if the value of ω is increased to 1, this will still only represent 2% of the total value of g . Thus it can be concluded that the effects of the gyroscopic precession will be negligible to the stability control and hence will be no cause for concern. Last years group experimentally determined the gyroscopic precession to be approximately 0.3 rad s^{-1} [6] and hence this is the value that shall be used for ω from this point forward.

Substituting the values from Table 2 into Equation 33 then gives:

$$\frac{\Theta(s)}{T(s)} = \frac{0.5}{1.05 \cdot s^2 + 0.5 \cdot s + 16.06} \quad \text{Equation 34}$$

5.4 Comparison of the linear and non linear equations

To enable a comparison between the linear and non linear systems Equation 21 was solved numerically in MathCAD using the fourth order Runge-Kutta method. 1000 iterations were specified to be carried out for each time step to ensure accurate results from the equation would be yielded. Finally a plot of the angular displacement against time was created and is shown in Figure 11.

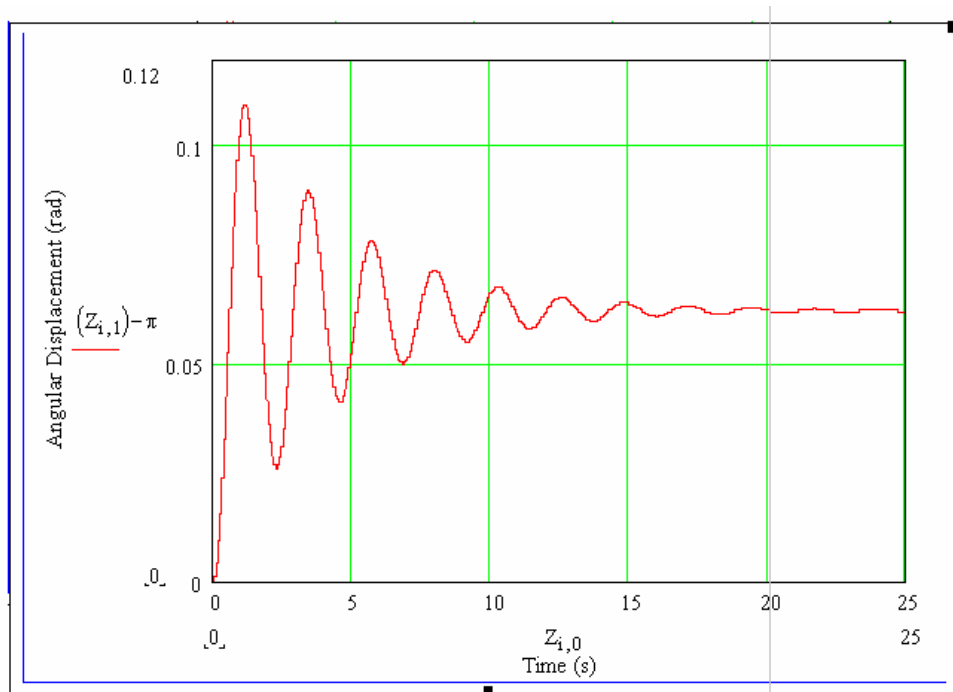


Figure 11: shows the step response to the non linear numerical solution

The transfer function, Equation 34, was inserted into Matlab, and the step response of the platform observed. Figure 12 shows a graph of the angular displacement against the time.

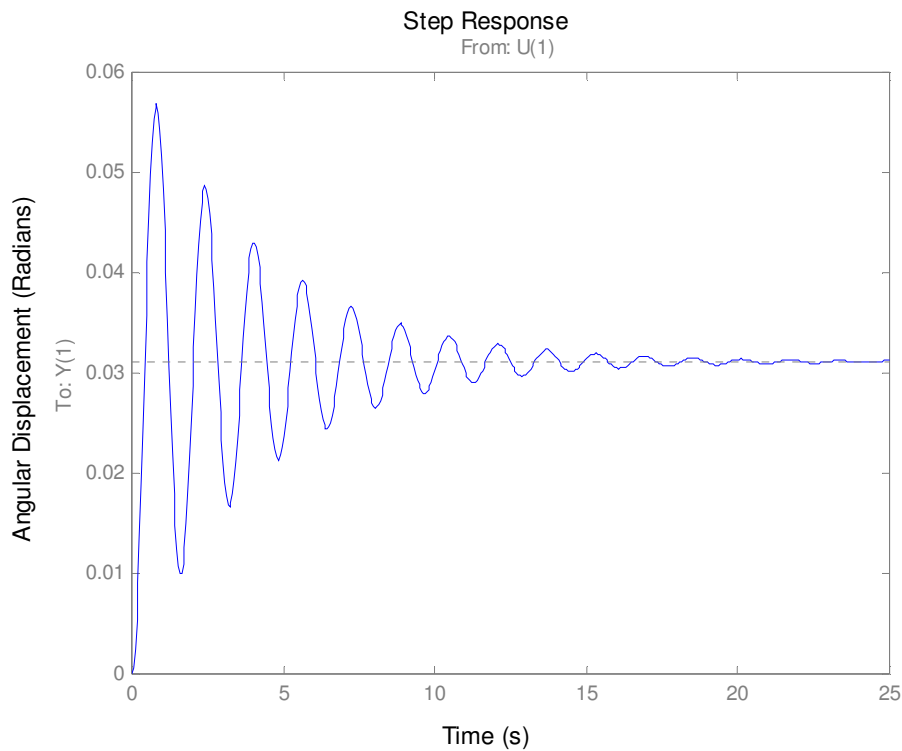


Figure 12: shows the step response to the linear solution

To allow a clearer comparison to be made between Figures 11 and 12 various system specifications were determined from each of the graphs and have been recorded in Table 3.

Table 3: Comparison of the linear & non linear system parameters

	Non Linear Results	Linearised Results
Steady state error $e(\infty)$	0.0621	0.0311
Settling Time (T_s)	15.94 s	16.20 s
Rise Time (T_r)	0.576 s	0.256 s
Peak Time (T_p)	1.140 s	0.819 s
Natural Frequency (ω_n)	2.75 Hz	4.0 Hz
Damping ratio (ζ)	0.091	0.062

As expected the non linear result, which includes the drag force, has a higher damping ratio, which accounts for all the other differences observed when comparing the other system parameters in Table 3. However the results produced by both methods are similar enough to allow the linearised model to be used to accurately represent the system.

5.5 Fan Transfer Function

To determine the transfer function for the perimeter fans a relationship of thrust against time must be determined for a step change in voltage. Once the control circuitry has been constructed the pulse width signal will be controlled by a linear relationship with voltage. As this linear relationship is known it can be incorporated in the block diagram in Figure 13 to form the overall transfer function of the fan.

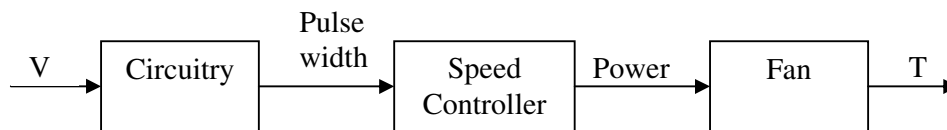


Figure 13: Block diagram representing the overall fan transfer function

To determine the relationship of thrust with time for a step change in voltage the first stage was to plot a graph of fan speed against time for a 10% step change in pulse width. The quadratic relationship determined in section 3.4.2 from the graph in Figure C2 relating the thrust to the fan speed can then be used to calculate the relationship of thrust with time for a step change in pulse width.

The final stage will then be to relate the step change in pulse width directly to a step change in voltage. As there is a linear relationship between pulse width and voltage where 0 V = 1.0 ms (equivalent of stop signal) and 5 V = 2.0 ms (equivalent full speed signal) a direct relationship between thrust and time can be found for a step change in voltage, thus enabling the transfer function to be determined.

To find the initial relationship between fan speed and time for a step change in pulse width the same method was used as described in experiment 3. On this occasion the readings from the voltage output from the frequency voltage converter were taken at

0.01 s intervals. This voltage was then converted to a fan speed and then finally a thrust. A graph of the thrust against time was then created and can be seen below in Figure 14.

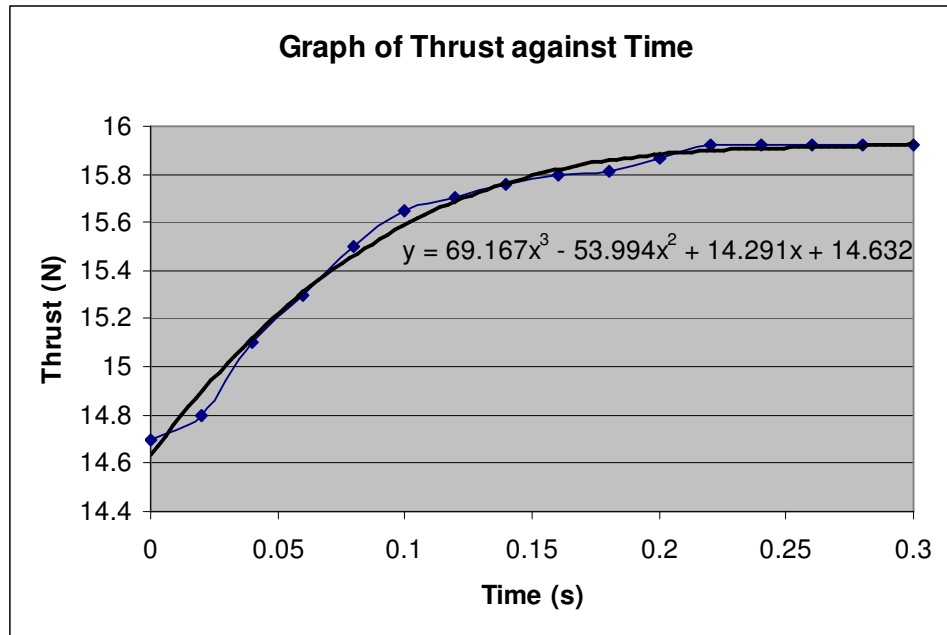


Figure 14: Graph of thrust against time

To simplify the transfer function the polynomial trend line can be approximated by an exponential curve of the form:

$$T = \beta \cdot (1 - e^{-Rt}) \quad \text{Equation 35}$$

Where: β = steady state value of the increment in thrust
 R = a constant

As the steady state value of thrust was 15.927 N and the initial thrust was 14.632 N the actual value for the steady state thrust, β , was:

$$\beta = 15.927 - 14.632 \rightarrow 1.295 \quad \text{Equation 36}$$

The constant, R was then determined by substituting in values from the equation of the line, e.g.

When $t = 0.29$, $T = 15.922$, $\beta = 1.295$, hence from Equation 34, $R = 18.27$

Thus substituting the values for β and R into Equation 35 produces Equation 37:

$$T = 1.295 \cdot (1 - e^{-18.27t}) \quad \text{Equation 37}$$

It was decided that a general closed loop transfer function should be constructed so that in the event of various parameters, such as the mass of the platform, being changed, the overall transfer function would not have to be completely recalculated each time. This would obviously require the construction of a block diagram expressed in general terms and has been shown in Figure 16.

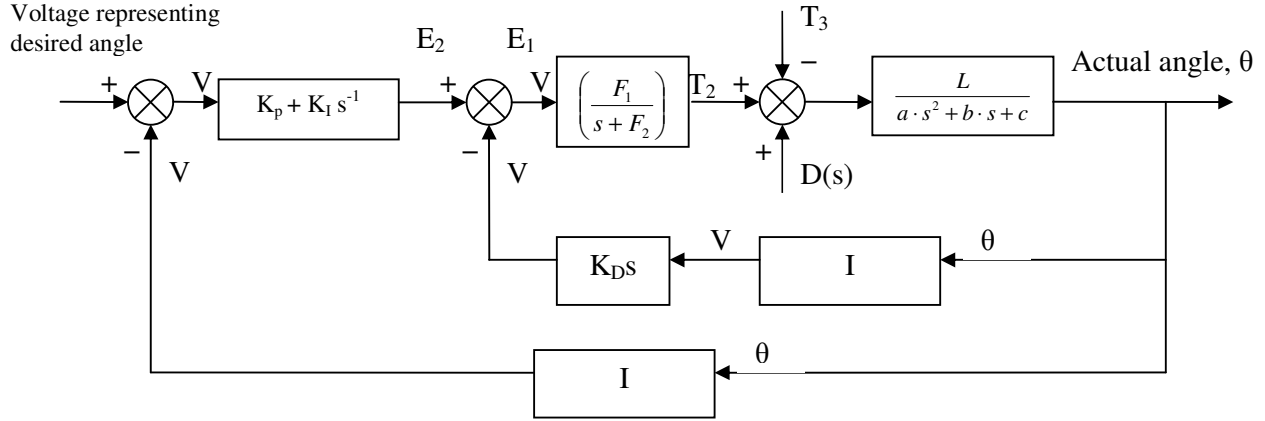


Figure 16: General form of the block diagram

The closed loop transfer function was then formed in stages. The first stage was to form the transfer function relating E_1 to the actual angle as follows:

$$\frac{\Theta(s)}{E_1(s)} = \frac{\frac{F_1}{s + F_2} \left(\frac{L}{a \cdot s^2 + b \cdot s + c} \right)}{1 + \frac{F_1}{s + F_2} \left(\frac{L}{a \cdot s^2 + b \cdot s + c} \right)} \quad \text{Equation 41}$$

$$\frac{\Theta(s)}{E_1(s)} = \frac{F_1 \cdot L}{a \cdot s^3 + (a \cdot F_2 + b)s^2 + (b \cdot F_2 + c)s + c \cdot F_2 + F_1 \cdot L} \quad \text{Equation 42}$$

Equation 42 was then used in forming the second stage of the transfer function which is the relationship between E_2 and the actual angle as follows:

$$\frac{\Theta(s)}{E_2(s)} = \frac{\frac{F_1 \cdot L}{a \cdot s^3 + (a \cdot F_2 + b)s^2 + (b \cdot F_2 + c)s + c \cdot F_2 + F_1 \cdot L}}{1 + \frac{F_1 \cdot L}{a \cdot s^3 + (a \cdot F_2 + b)s^2 + (b \cdot F_2 + c)s + c \cdot F_2 + F_1 \cdot L} (K_D \cdot s \cdot I)} \quad \text{- Equation 43}$$

$$\frac{\Theta(s)}{E_2(s)} = \frac{F_1 \cdot L}{a \cdot s^3 + (a \cdot F_2 + b)s^2 + (b \cdot F_2 + c + F_1 \cdot I \cdot K_D \cdot L)s + c \cdot F_2 + F_1 \cdot L} \quad \text{- Equation 44}$$

Finally the overall transfer function was formed using Equation 44, to find a relationship between the input voltage representing the desired angle and the actual angle as follows:

$$\frac{\Theta(s)}{V(s)} = \frac{(K_p + K_I \cdot s^{-1}) \left(\frac{F_1 \cdot L}{a \cdot s^3 + (a \cdot F_2 + b)s^2 + (b \cdot F_2 + c + F_1 \cdot I \cdot K_D \cdot L)s + c \cdot F_2 + F_1 \cdot L} \right)}{1 + (K_p + K_I \cdot s^{-1}) \left(\frac{F_1 \cdot L}{a \cdot s^3 + (a \cdot F_2 + b)s^2 + (b \cdot F_2 + c + F_1 \cdot I \cdot K_D \cdot L)s + c \cdot F_2 + F_1 \cdot L} \right)} \cdot I$$

- Equation 45

$$\frac{\Theta(s)}{V(s)} = \frac{L \cdot F_1 \cdot K_p \cdot s + L \cdot F_1 \cdot K_I}{a \cdot s^4 + (a \cdot F_2 + b)s^3 + (b \cdot F_2 + c + F_1 \cdot I \cdot K_D \cdot L)s^2 + (c \cdot F_2 + F_1 \cdot L + F_1 \cdot I \cdot K_p \cdot L)s + F_1 \cdot I \cdot K_I \cdot L}$$

- Equation 46

The constants F_1 , F_2 , a , b , c , and I , can now be related back to the first block diagram in Figure 15. Substituting in the appropriate values will then yield the overall closed loop transfer function as:

$$\frac{\Theta(s)}{V(s)} = \frac{5.915 \cdot K_p \cdot s + 5.915 \cdot K_I}{1.05 \cdot s^4 + 19.68s^3 + (25.2 + 84.71 \cdot K_D)s^2 + (299.33 + 84.71 \cdot K_p)s + 84.71 \cdot K_I}$$

- Equation 47

5.8 Routh-Hurwitz Stability Criterion, Bode & Nyquist plots

The Routh-Hurwitz criterion states that the number of roots of the characteristic equation, $q(s)$, with positive real parts is equal to the number of changes in sign of the first column of the Routh arrays. This simply means that for a system to be stable all values in the first column of the Routh array must be positive. This can be used to help determine the range of values for the system parameters K_D , K_I , and K_p . The characteristic equation for this system is taken directly from the denominator of Equation 47, giving:

$$q(s) = 1.05 \cdot s^4 + 19.68s^3 + (25.2 + 84.71 \cdot K_D)s^2 + (299.33 + 84.71 \cdot K_p)s + 84.71 \cdot K_I$$

- Equation 48

This can then be used to form the following Routh array:

$$\begin{array}{c|ccc} s^4 & 1.05 & 25.2 + 84.71 \cdot K_D & 84.71 \cdot K_I \\ s^3 & 19.68 & 299.33 + 84.71 \cdot K_p & 0 \\ s^2 & b_2 & b_0 & 0 \\ s & c_1 & 0 & 0 \\ s^0 & d_0 & 0 & 0 \end{array}$$

The general equation used to solve the unknown constants in the Routh array can be found in Appendix J.

Using the general equations given in Appendix J the constants b_2 , b_0 , c_1 and d_0 can be determined as follows:

$$b_2 := \frac{-1}{19.68} \cdot \left| \begin{pmatrix} 1.05 & 25.2 + 84.71K_D \\ 19.68 & 299.33 + 84.71K_P \end{pmatrix} \right| \quad \text{Equation 49}$$

$$b_2 = 9.23 - 4.52 \cdot K_P + 84.71 \cdot K_D \quad \text{Equation 50}$$

$$b_0 := \frac{-1}{19.68} \cdot \left| \begin{pmatrix} 1.05 & 84.71K_I \\ 19.68 & 0 \end{pmatrix} \right| \quad \text{Equation 51}$$

$$b_0 = 84.71 \cdot K_I \quad \text{Equation 52}$$

$$c_1 := \frac{-1}{b_2} \cdot \left| \begin{pmatrix} 19.68 & 299.33 + 84.71K_P \\ b_2 & b_0 \end{pmatrix} \right| \quad \text{Equation 53}$$

$$c_1 = \frac{(-3333989 \cdot K_I + 2721.305 - 1248056 \cdot K_P + 51703932 \cdot K_D - 1531.237 \cdot K_P^2 + 28699748 \cdot K_P \cdot K_D)}{8.916 - 9.039 \cdot K_P + 169.41 \cdot K_D} \quad \text{- Equation 54}$$

$$d_0 := \frac{-1}{c_1} \cdot \left| \begin{pmatrix} b_2 & b_0 \\ c_1 & 0 \end{pmatrix} \right| \quad \text{Equation 55}$$

$$d_0 = 84.71 \cdot K_I \quad \text{Equation 56}$$

The only easily determined controller value from these equations is the value of $K_I \geq 0$. Due to the complexity of trying to solve a range of values for this fourth order system, it was decided to set $K_I = 0$ so the system would now be controlled by a minor loop PD controller. This then simplified the coefficients of the Routh-Hurwitz stability criterion to give the constants as follows:

$$b_2 = 9.23 - 4.52 \cdot K_P + 84.71K_D \quad \text{Equation 57}$$

$$c_1 = 299.33 + 84.71 \cdot K_P \quad \text{Equation 58}$$

Equations 57 and 58 could then be rearranged to give the range of values for K_P and K_D as follows:

$$K_P > \frac{-299.33}{84.71} \Rightarrow -3.52 \quad \text{Equation 59}$$

$$K_D < \frac{-25.14}{84.71} \Rightarrow -0.297 \quad \text{Equation 60}$$

5.9 System specifications

There are 4 main specifications that must be considered when controlling the response of a system. These are the steady state error, the rise time, the percentage overshoot, and the settling time.

The steady state error, $e(\infty)$, of a system is defined as the difference between the required (desired) output signal and the actual output signal. Obviously the smaller this value is the better. For this system a steady state error of less than 1° (0.0175 radians) has been specified.

The rise time, T_r , is the most important system specification as it will ultimately determine whether or not the system can be controlled. The rise time is the time required for the response to go from 0% to 100% of its final value. For the system to be controlled the rise time must be greater than the response time of the fans. The response time of the fans for a worst case scenario had previously been determined as 0.3 s. Consequently it was decided to specify the rise time as being greater than 0.6 s.

The percentage overshoot is the next system specification considered. This is defined as the maximum amount by which the system output response proceeds beyond the desired response. Again the lower this value is the better, ideally the system would be critically damped meaning the percentage overshoot would be 0. However it has been decided that a percentage overshoot of less than 5% will be acceptable.

The final consideration with regard to the system specification is the settling time. This is the time required for the system output to settle within a certain percentage of the input amplitude, which in this case has been defined as 2%. The settling time is not overly important within the system specifications however it is hoped a settling time of less than 10 s can be achieved, preferably closer to 5 s. The settling time should not be too short however, as this will result in rather jerky restoring moments produced by the perimeter fans, a smoother return to the equilibrium position would be preferential.

A summary of these specifications has been given in Table 4 below.

Table 4: System specifications

The Steady State Error, $e(\infty)$	$< 1^\circ \approx 0.0175$ radians
Rise Time, T_r	> 0.6 s
Percentage Overshoot	$< 5\%$
Settling Time, T_s	< 10 s

5.10 Controller Design

The control system is made up of 3 controllers, K_I , K_P , and K_D . These are known as the integral control, the proportional control and the derivative control respectively. Each of the terms has a specific affect on the system response.

Table 5 shows the affects each controller has on the system.

Table 5: Affect of controllers on the system response

Controller	Rise Time (T_r)	Percentage Overshoot	Settling Time (T_s)	Steady State Error, $e(\infty)$
K_P	Decrease	Increase	Small Change	Decrease
K_I	Decrease	Increase	Small Change	Eliminate
K_D	Small Change	Decrease	Decrease	Small Change

The controller values were determined by inserting equation 47 into Matlab and ascertaining the response for a step input. The controller values were then altered using a logical iterative process. The system specification values for each iteration have been recorded in Table 6.

Table 6: Controller values attempted and the corresponding system responses produced.

Controller Values	Steady State Error, $e(\infty)$	Rise Time (T_r)	Percentage Overshoot	Settling Time (T_s)
$K_P = 2$ $K_D = 50$	0.0367	29	0	51.6
$K_P = 2$ $K_D = 25$	0.0367	14.5	0	25.9
$K_P = 2$ $K_D = 8$	0.0367	4.67	0	8.34
$K_P = 1$ $K_D = 8$	0.0249	6.36	0	11.3
$K_P = 0.5$ $K_D = 8$	0.0152	7.75	0	13.8
$K_P = 0.5$ $K_D = 4$	0.0152	3.91	0	6.96
$K_P = 0.25$ $K_D = 4$	0.00851	4.38	0	7.82
$K_P = 0.25$ $K_D = 2$	0.00851	2.16	0	3.93
$K_P = 0.25$ $K_D = 3$	0.00851	3.29	0	5.89
$K_P = 0.1$ $K_D = 3$	0.00367	3.56	0	6.36
$K_P = 0.05$ $K_D = 3$	0.00189	3.66	0	6.54

The final values decided upon for the controllers are as follows: $K_I = 0$, $K_P = 0.05$, $K_D = 3$. These values have been highlighted in Table 6 above so their effective responses on the system can easily be seen. Figure 17 shows the step response, and allows a clearer visualisation of what the system specification values actually relate to.

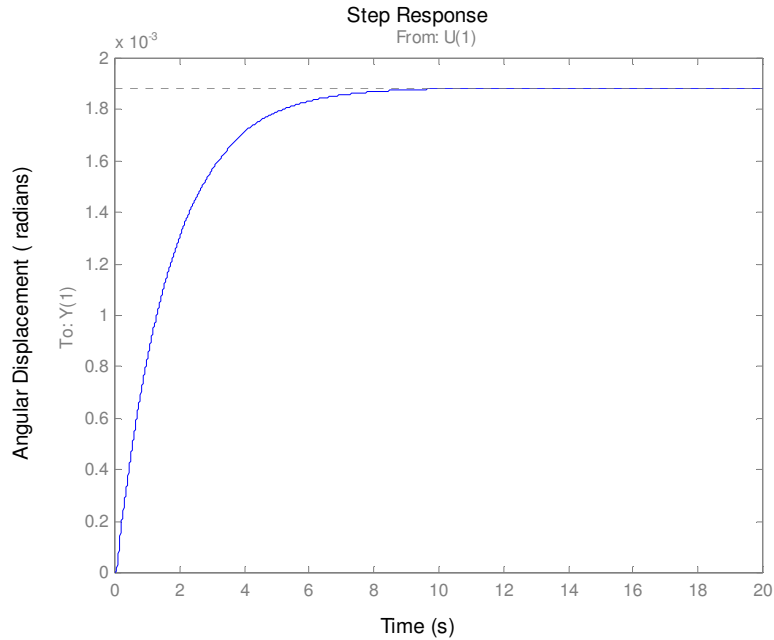


Figure 17: Step response of the system

Once the required response was produced by the controllers other inputs were tried and their responses on the system observed. The most important response observed was the impulse response which has been shown below in Figure 18. When an impulse is inputted into the system it is some what analogous to a sudden gust of wind. For this reason it is useful to see how the platform will respond. On looking at Figure 18 it can be concluded that the platform responds rather well, and it is thought once the control system has been tested in reality the stability control will prove to be very successful.

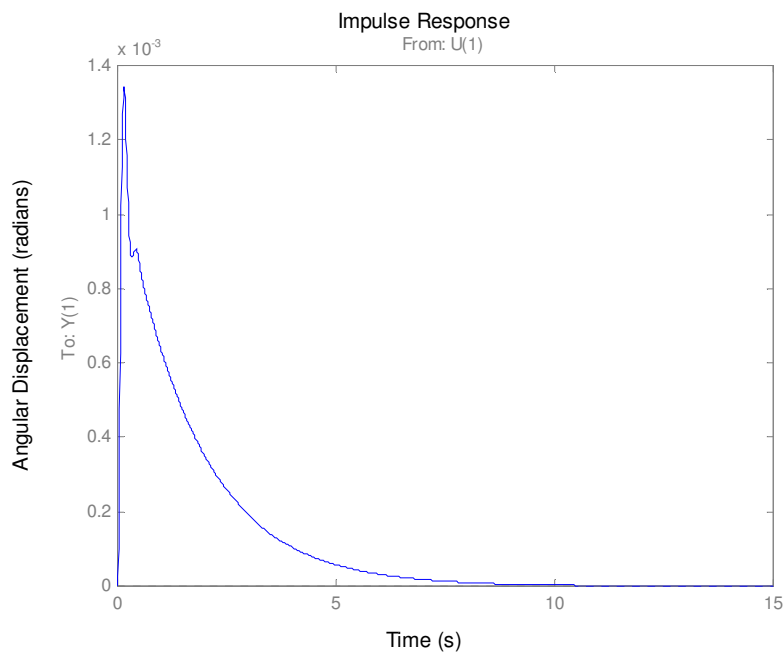


Figure 18: Impulse Response of the system

6. Height Control

6.1 Mathematical Model

The height control system can be simply represented by the diagram shown in Figure 19.

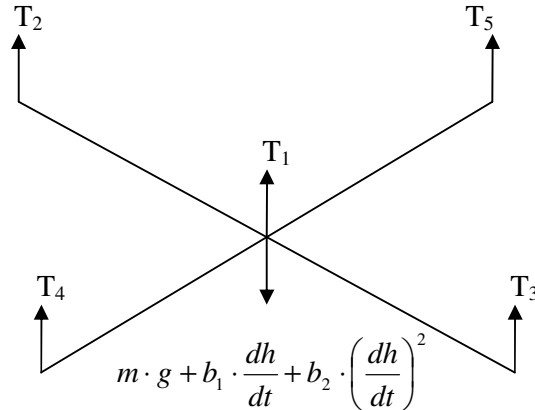


Figure 19: Free body diagram of the platform

When the platform is in equilibrium the following force balance can be made:

$$T_1 + T_2 + T_3 + T_4 + T_5 = m \cdot g + b_1 \cdot \frac{dh}{dt} + b_2 \cdot \left(\frac{dh}{dt}\right)^2 \quad \text{Equation 61}$$

Initially it was hoped that the central fan would be used to control the height, with the perimeter fans controlling the stability. However after extensive testing was carried out by Richard Holbrook [8], the following factors were revealed.

- The amount of thrust that the central fan had been detailed to achieve had been grossly overestimated, and the maximum amount of thrust actually generated during testing was 50 N (5.1 kg).
- The throttle control of the central fan proved to be unreliable, resulting in unpredictable responses from the fan.

As a result of these two factors it was decided that the central fan could not be used to control the height. The central fan was now to be run at a constant speed producing the maximum amount of thrust possible, which for the control design shall be taken as a constant value of 50 N of thrust.

Combining the height and stability control to be carried out by the perimeter fans should not be too complex, as the height signal can simply be added to the stability control signal. For an overall block diagram of the combined system in one axis see Appendix K.

Now these design constraints have been determined the mathematical model for one perimeter fan can be developed as follows:

The central fan can be assumed to produce 50 N of thrust, with the four perimeter fans distributing the remainder of thrust required equally between them. Incorporating this information into Equation 61 will then produce Equation 62 as follows:

$$\frac{T_1}{4} + 4 \cdot T_C - m \cdot g - b_1 \cdot \frac{dh}{dt} - b_2 \left(\frac{dh}{dt} \right)^2 = 0 \quad \text{Equation 62}$$

Where: $T_C = T_1 = T_2 = T_3 = T_4$

This then allows the force balance for one perimeter fan to be expressed in Equation 63.

$$T_C + \frac{T_1}{4} - \frac{m \cdot g}{4} - \frac{b_1}{4} \cdot \frac{dh}{dt} - \frac{b_2}{4} \cdot \left(\frac{dh}{dt} \right)^2 = 0 \quad \text{Equation 63}$$

Equating Equation 63 to Newton's second law then yields the following final equation representing the mathematical model in general terms:

$$T_C + \frac{T_1}{4} - \frac{m \cdot g}{4} = m \cdot \left(\frac{d^2h}{dt^2} \right) + \frac{b_1}{4} \left(\frac{dh}{dt} \right) + \frac{b_2}{4} \left(\frac{dh}{dt} \right)^2 \quad \text{Equation 64}$$

6.2 Linearisation

From the mathematical model determined in Equation 64, it can be seen that there is only one non linear term requiring linearisation. This term is the drag force. As with the stability control when this term is linearised it goes to 0. Yielding the complete linearised equation as:

$$T_C + \frac{T_1}{4} - \frac{m \cdot g}{4} = m \cdot \left(\frac{d^2h}{dt^2} \right) + \frac{b_1}{4} \left(\frac{dh}{dt} \right) \quad \text{Equation 65}$$

In section 5.4 it was concluded that the neglect of the drag force term in the linearised equation still produced a valid representation of the model. Consequently it can also be concluded that the linearised equation, Equation 65, will also be valid. The values for the known terms in Equation 65 have been expressed in Table 7.

Table 7: Design parameters

Thrust produced by central fan, T_1	50 N
Mass, m	8.17 kg
Coefficient of friction, b_1	0.5

Substituting the values from Table 7 into Equation 65 gives the following:

$$T_C - 7.54 = m \cdot \left(\frac{d^2h}{dt^2} \right) + \frac{b_1}{4} \cdot \left(\frac{dh}{dt} \right) \quad \text{Equation 66}$$

6.3 Transfer Function

Taking the Laplace transform of Equation 66 gives the transfer function for height control for one perimeter fan as follows:

$$T(s) = m \cdot s^2 \cdot H(s) + \frac{b_1}{4} \cdot \frac{dh}{dt} \quad \text{Equation 67}$$

Rearranging Equation 67 then gives the general equation for the transfer function as follows:

$$\frac{H(s)}{T(s)} = \frac{1}{m \cdot s^2 + \frac{b_1}{4} \cdot s} \quad \text{Equation 68}$$

Substituting the known values from Table 7 into Equation 68 then gives:

$$\frac{H(s)}{T(s)} = \frac{1}{8.17 \cdot s^2 + 0.125 \cdot s} \quad \text{Equation 69}$$

Simulating the impulse response of this transfer function in Matlab yielded the graph shown in Figure 20. The graph shows the system to be stable, however there is no control to stabilise the platform at the correct height. As the controllers have not yet been introduced this is to be expected.

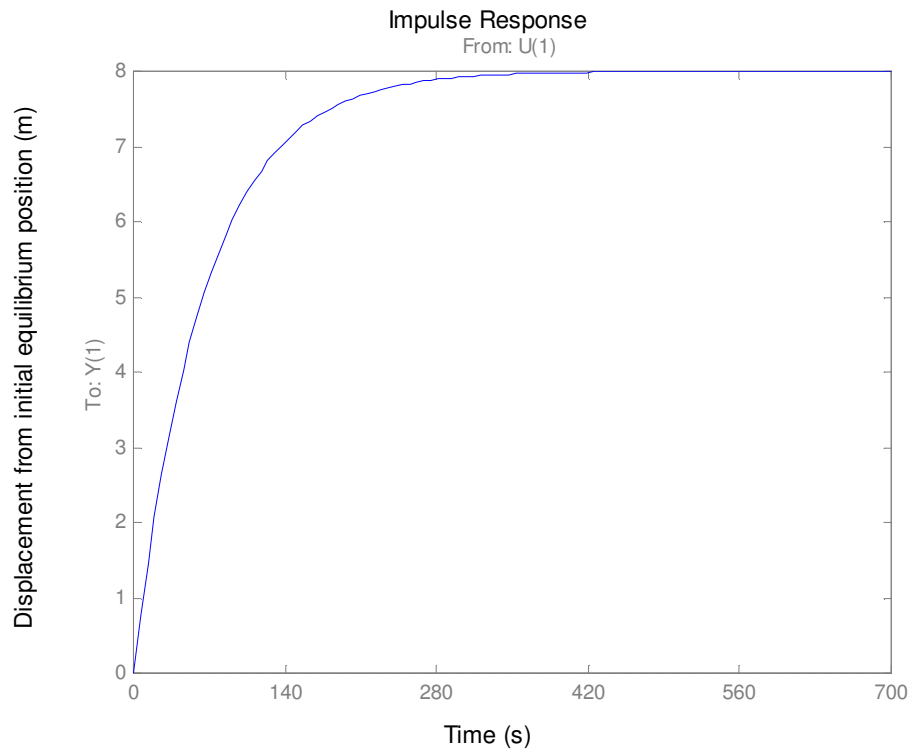


Figure 20: Impulse response of the height transfer function

6.4 Fan and IMU Transfer Function

As the perimeter fans are used for control of the height instead of the central fan the transfer function determined in section 5.5 will be used.

The IMU transfer function for height control proved problematic. Richard Forder experienced problems when using the IMU to measure the height. Consequently a relationship between the height measured and the voltage output from the IMU were unable to be determined. On discussing this problem with Richard Forder, it was decided an assumed relationship of 1V per metre should be taken. Once the actual relationship has been determined Richard mentioned that the output could easily be scaled to match the assumed relationship. Hence the IMU transfer function can be represented by the following simple gain:

$$\frac{V(s)}{H(s)} = 1 \quad \text{Equation 70}$$

6.5 Overall Block Diagram of the Height Control

The general overall block diagram for the height control has been represented below in Figure 21.

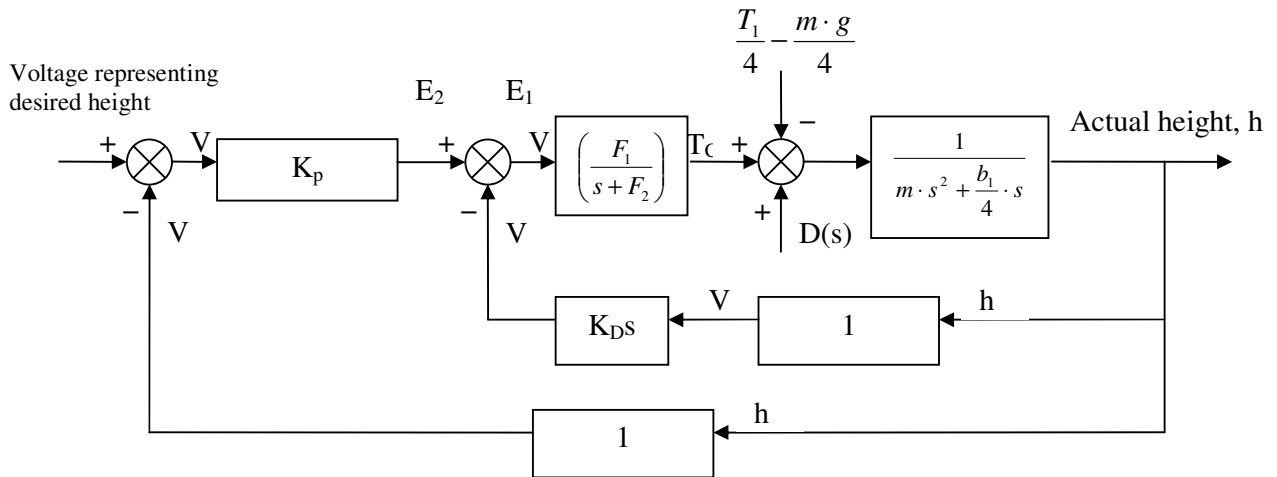


Figure 21: Block diagram of the height control system

This was then used to create the overall closed loop transfer function in stages. The first stage was to form the transfer function relating E_1 to the actual height as follows:

$$\frac{H(s)}{E_1(s)} = \frac{\frac{F_1}{s + F_2} \left(\frac{1}{m \cdot s^2 + b \cdot s} \right)}{1 + \frac{F_1}{s + F_2} \left(\frac{1}{m \cdot s^2 + b \cdot s} \right)} \quad \text{Equation 71}$$

Where $b = \frac{b_1}{4}$

$$\frac{H(s)}{E_1(s)} = \frac{F_1}{m \cdot s^3 + (b + m \cdot F_2) \cdot s^2 + b \cdot F_2 \cdot s + F_1} \quad \text{Equation 72}$$

Equation 72 was then used in forming the second stage of the transfer function which is the relationship between E_2 and the actual height as follows:

$$\frac{H(s)}{E_2(s)} = \frac{\frac{F_1}{m \cdot s^3 + (b + m \cdot F_2) \cdot s^2 + b \cdot F_2 \cdot s + F_1}}{1 + \frac{F_1}{m \cdot s^3 + (b + m \cdot F_2) \cdot s^2 + b \cdot F_2 \cdot s + F_1} (K_D \cdot s)} \quad \text{Equation 73}$$

$$\frac{H(s)}{E_2(s)} = \frac{F_1}{m \cdot s^3 + (b + m \cdot F_2) \cdot s^2 + (b \cdot F_2 + F_1 \cdot K_D) \cdot s + F_1} \quad \text{Equation 74}$$

Finally the overall transfer function was formed using Equation 74, to form a relationship between the actual height and the voltage representing the desired height as follows:

$$\frac{H(s)}{V(s)} = \frac{\frac{F_1}{m \cdot s^3 + (b + m \cdot F_2) \cdot s^2 + (b \cdot F_2 + F_1 \cdot K_D) \cdot s + F_1} (K_p)}{1 + \frac{F_1}{m \cdot s^3 + (b + m \cdot F_2) \cdot s^2 + (b \cdot F_2 + F_1 \cdot K_D) \cdot s + F_1} (K_p)}$$

- Equation 75

$$\frac{H(s)}{V(s)} = \frac{F_1 \cdot K_p}{m \cdot s^3 + (b + m \cdot F_2) \cdot s^2 + (b \cdot F_2 + F_1 \cdot K_D) \cdot s + F_1 + F_1 \cdot K_p}$$

- Equation 76

The appropriate values were then substituted into Equation 76 to yield the overall height transfer function as:

$$\frac{H(s)}{V(s)} = \frac{11.83 \cdot K_p}{8.17 \cdot s^3 + 149.39 \cdot s^2 + (2.28 + 11.83 \cdot K_D) \cdot s + 11.83 + 11.83 \cdot K_p}$$

- Equation 77

6.6 Routh-Hurwitz Stability Criterion

Ensuring Equation 77 meets the Routh-Hurwitz stability criterion as previously explained in section 5.8 reveals the following range of values for the controllers K_P and K_D as:

$$\begin{array}{l|ll} s^3 & 8.17 & 2.28 + 11.83 \cdot K_D \\ s^2 & 149.39 & 11.83 + 11.83 \cdot K_P \\ s & e_1 & 0 \\ s^0 & f_0 & 0 \end{array}$$

$$e_1 := \frac{-1}{149.39} \cdot \left[\begin{array}{cc} 8.17 & 2.28 + 11.83 K_D \\ 149.39 & 11.83 + 11.83 K_P \end{array} \right]$$

$$f_0 := \frac{-1}{e_1} \cdot \left[\begin{array}{cc} 149.39 & (11.83 + 11.83 K_P) \\ e_1 & 0 \end{array} \right]$$

$$e_1 = 1.633 - 0.647 \cdot K_P + 11.83 \cdot K_D$$

$$f_0 = 11.83 + 11.83 \cdot K_P$$

$$K_D > -0.19$$

$$K_P > -1$$

6.7 System specifications

As previously discussed in chapter 5 there are 4 main system specifications that must be determined prior to designing the controller. For the height control the following specifications were decided upon.

Taking into account the platform is to hover at a constant height of 1 m above ground level it was decided that the steady state error should be less than 2 cm. The smaller the value of the steady state error produced the more effective the height control will be.

The rise time as previously specified in chapter 5 must be slower than the response time of the fans in order for the system to be controlled. Hence as the response time in a worst case scenario was determined to be 0.3 s, it was decided the rise time should exceed a value of 0.6 s.

The percentage overshoot should be as low as possible and must be below 5%. A critically damped system would again be preferable.

The settling time is not overly important, but has been decided to be less than 20 s, but preferably closer to 10 s. These specifications have been summarised in Table 8 below.

Table 8: System specifications for height control

The Steady State Error, $e(\infty)$	< 2 cm
Rise Time, Tr	> 0.6 s
Percentage Overshoot	< 5%
Settling Time, Ts	< 20 s

6.8 Controller Design

The control system for the height control was made up of 2 controllers, K_P , and K_D . These are known as the proportional controller, and the derivative controller respectively. Each of the terms has a specific affect on the system response which has been shown in Table 5

It was decided to test the system response with a unit step input at first and iteratively determine the values of K_D , and K_P . The system specifications determined for each iteration have been recorded in Table 9 below.

Table 9: Controller values attempted with their corresponding affect on the system specifications

Controller Values	Steady State Error, $e(\infty)$	Rise Time (T_r)	Percentage Overshoot	Settling Time (T_s)
$K_P = 1$ $K_D = 10$	0.5	8.57	0	15.1
$K_P = 0.5$ $K_D = 10$	0.333	12.2	0	22.2
$K_P = 0.01$ $K_D = 10$	0.0099	19.4	0	35.4
$K_P = 0.01$ $K_D = 5$	0.0099	7.74	3.88	20.6
$K_P = 0.01$ $K_D = 6$	0.0099	9.61	0.4	15.4
$K_P = 0.01$ $K_D = 5.5$	0.0099	8.61	1.98	13.1
$K_P = 0.01$ $K_D = 5.4$	0.0099	8.42	2.02	12.8
$K_P = 0.01$ $K_D = 4.3$	0.0099	8.24	2.02	19.1

The final values decided upon for the controllers are as follows: $K_P = 0.01$, $K_D = 4.3$. These values have been highlighted in Table 9 above so their effective responses on the system can easily be seen. Figure 22 overleaf shows the step response, and allows a clearer visualisation of what the system specification values actually relate to.

As the response of the system to a step input was successfully controlled, the response to an impulse was observed. Figure 23 overleaf shows a graph representing the impulse response.

From Figures 22 and 23 it can be concluded that the steady state is within, the required boundaries, and that the system is close to behaving as if it were critically damped. The rise time is also more than adequate. The only system specification which could be improved upon is the settling time. The settling time is still within the specifications determined in Table 8, however a value closer to 10 s would have been preferred. The reason a lower value for the settling has not been reached is simply because the PD controller had reached the limit to how much the settling time could be reduced if the other system specifications were to be met.

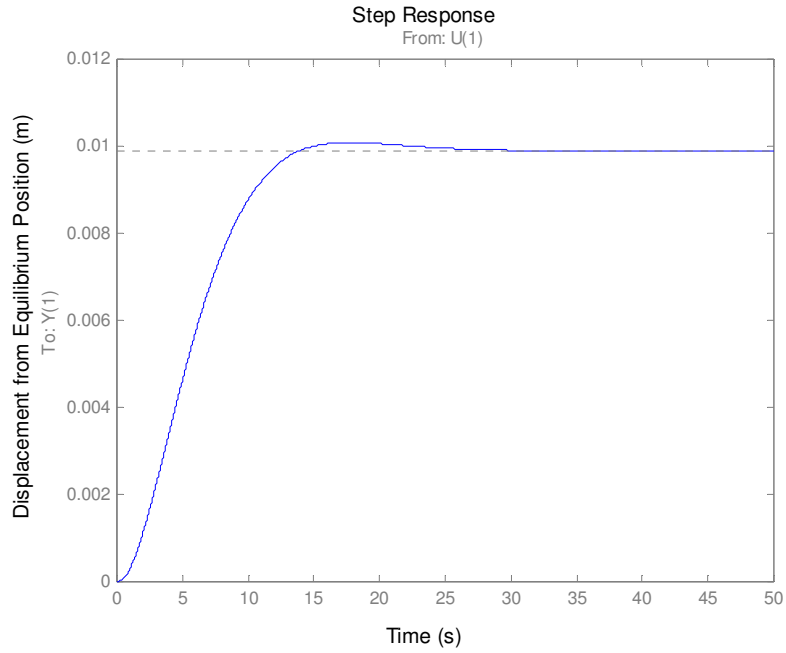


Figure 22: Step response of the system

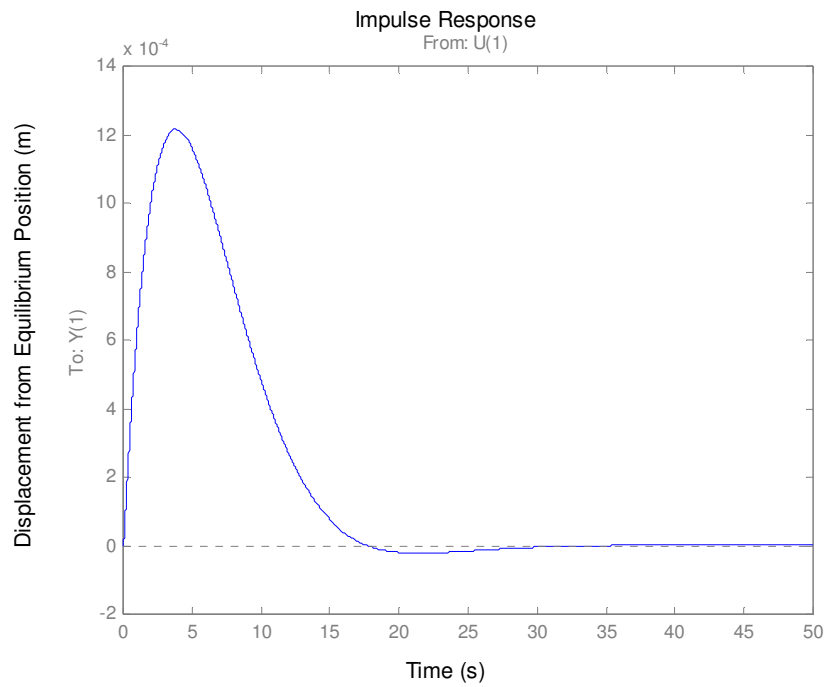


Figure 23: Impulse response to the system

7. Final Conclusions, Discussion & Further Work

The testing carried out on the perimeter fans was a success, allowing the system parameters determined from the test results to be accurately incorporated within the control system.

The development of the control theory was also very successful. The linear models were validated against the non linear models, proving that the linearised equations were effective in representing the control system. The controllers were also proven to provide an adequate system response within the system specifications defined. This was proven using Matlab, and shows theoretically how the platform can be controlled.

On the whole the design and development of the flying platform encountered numerous problems predominantly with the central fan testing. This had a knock on effect to other parts of the project and hence the design and development of the structure was not completed. This meant certain vital system parameters with regard to the control had to be estimated, which was by no means ideal, however the general control theory was a success and it is hoped that before the presentation, a fully working model will be built, and incorporated within the presentation.

With regard to further work on the control system, the mathematical models must now be extended to allow for the control of horizontal flight and yaw. To allow the incorporation of horizontal flight, will require the addition of an onboard microprocessor. The flight data would then be loaded onto the microprocessor allowing the platform to start up, take off, complete its designated flight plan, and then land. It has also been suggested that a Global Positioning System (GPS) should be incorporated, in order that the platform can recognise its precise location. Once these remaining problems have been solved and incorporated into the flying platform, a completely autonomous flight system will have been developed.

Appendix A

The Product Design Specification

Table A1: The Product Design Specification	
Performance	<ol style="list-style-type: none"> 1. Must hover approximately 1 m above the ground. 2. Flight duration to be approximately 20 minutes. 3. Must remain Stable. 4. Must provide viable operating platform. 5. Must be able to carry a payload of up to 3 kg. 6. Must have the capability to have the On/Off controlled by remote.
Environment	<ol style="list-style-type: none"> 1. Must be capable of operating in a temperature range of -10°C to 50°C. 2. Must be capable of operating in humid conditions and to be water resistant when operating in light rain. 3. Must be operated in minimal air flow disturbances i.e. minimal wind speeds.
Maintenance	<ol style="list-style-type: none"> 1. Onboard battery must be easily attainable for possible replacement, and recharging. 2. Fuel tank for internal combustion engine must also be easily accessible for refuelling.
Life in Service	<ol style="list-style-type: none"> 1. Products life in service is to be approximately 5 years.
Target Production Cost	<ol style="list-style-type: none"> 1. A budget of £1000 has been assigned to this project.
Size	<ol style="list-style-type: none"> 1. The flying platforms dimensions to be similar to the dimensions specified in the previous groups report.
Weight	<ol style="list-style-type: none"> 1. Yet to be determined but should be designed for minimum weight possible. Estimated weight including payload is approx 10 kg.
Materials	<ol style="list-style-type: none"> 1. Materials used must have a high mechanical tolerance, and must have as low a density as possible.
Design Constraints	<ol style="list-style-type: none"> 1. The flight must be completely autonomous. 2. The design must not be a helicopter based design. 3. Must use an onboard IC engine for power generation.

Appendix B

Data and graphs for the Fan Speed Measurement

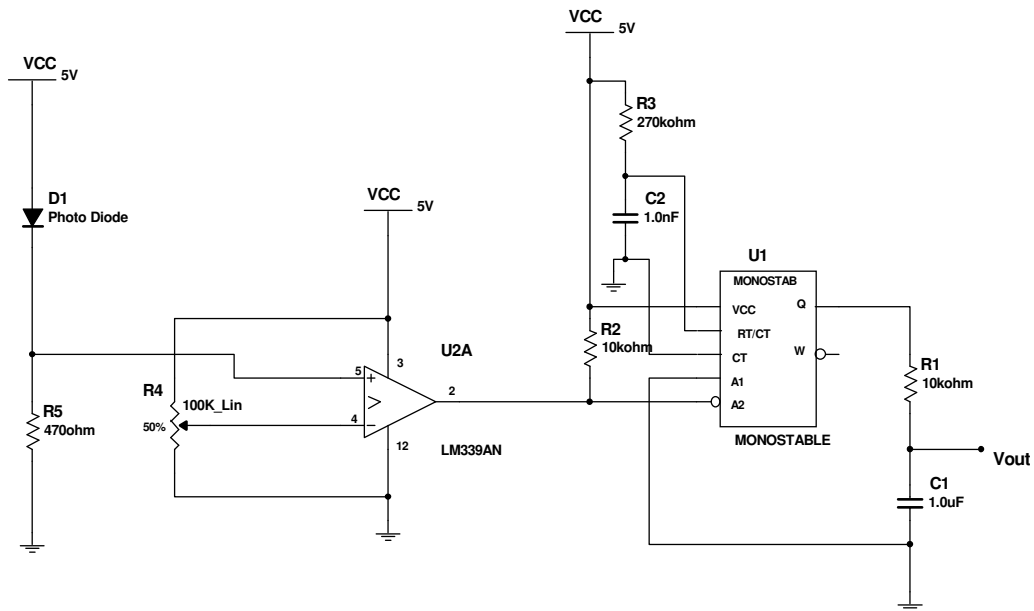


Figure B24: Circuit Diagram of the Frequency to Voltage Converter.

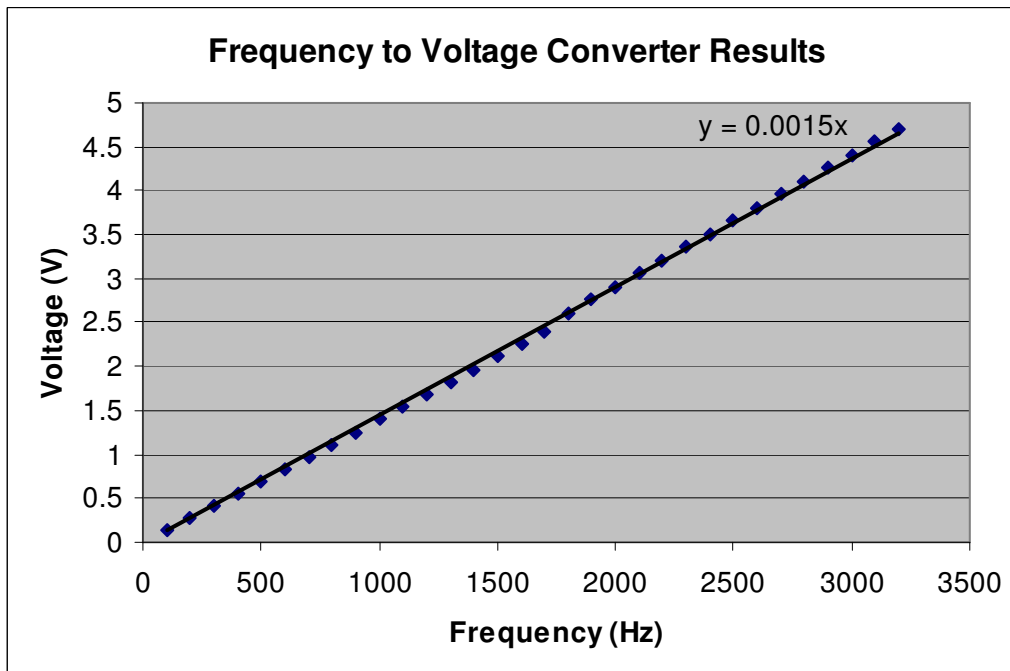


Figure B25: Graph of the voltage against frequency

Appendix C

Data and Graphs Produced From Test Results to Experiment 1

Table C10: Results to Experiment 1

Pulse Width (ms)	Voltage Output of Frequency Converter (V)	Frequency (Hz)	RPS	RPM	Current In (A)	Voltage In (V)	Power In (W)	Mass Reading (g)	Thrust (g)	Thrust (N)
1.00	0.00	0	0.00	0	0.0	25.4	0.0	0	0.00	0.00
1.07	0.72	480	80.00	4800	0.4	25.3	10.1	90	45.45	0.45
1.10	0.74	493	82.22	4933	0.5	25.2	12.6	90	45.45	0.45
1.15	1.05	700	116.67	7000	1.0	25.1	25.1	185	93.42	0.92
1.20	1.33	887	147.78	8867	1.8	25.0	45.0	325	164.11	1.61
1.25	1.57	1047	174.44	10467	2.7	24.9	67.2	455	229.75	2.25
1.30	1.80	1200	200.00	12000	3.6	24.8	89.3	630	318.12	3.12
1.35	2.04	1360	226.67	13600	4.8	24.7	118.6	765	386.29	3.79
1.40	2.23	1487	247.78	14867	6.8	24.6	167.3	945	477.18	4.68
1.45	2.50	1667	277.78	16667	9.0	24.5	220.5	1200	605.94	5.94
1.50	2.77	1847	307.78	18467	10.5	24.5	257.3	1420	717.03	7.03
1.55	2.97	1980	330.00	19800	13.3	24.3	323.2	1700	858.42	8.42
1.60	3.24	2160	360.00	21600	16.8	24.3	408.2	2000	1009.90	9.91
1.65	3.46	2307	384.44	23067	20.0	24.3	486.0	2300	1161.39	11.39
1.70	3.70	2467	411.11	24667	24.1	24.1	580.8	2620	1322.97	12.98
1.75	3.89	2593	432.22	25933	28.0	24.0	672.0	2925	1476.98	14.49
1.80	4.10	2733	455.56	27333	34.0	23.9	812.6	3280	1656.24	16.25
1.85	4.31	2873	478.89	28733	39.0	23.8	928.2	3600	1817.82	17.83
1.90	4.48	2987	497.78	29867	46.0	23.7	1090.2	3930	1984.46	19.47
1.95	4.57	3047	507.78	30467	48.0	23.7	1137.6	4120	2080.40	20.41
2.00	4.58	3053	508.89	30533	48.8	23.7	1156.6	4120	2080.40	20.41

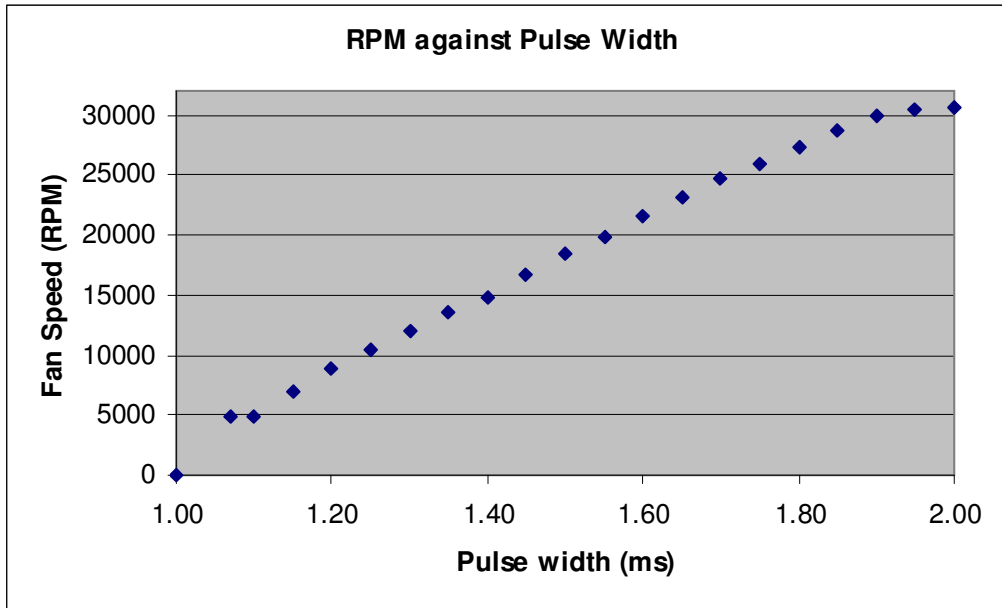


Figure C26: Graph of fan speed against the input pulse width signal

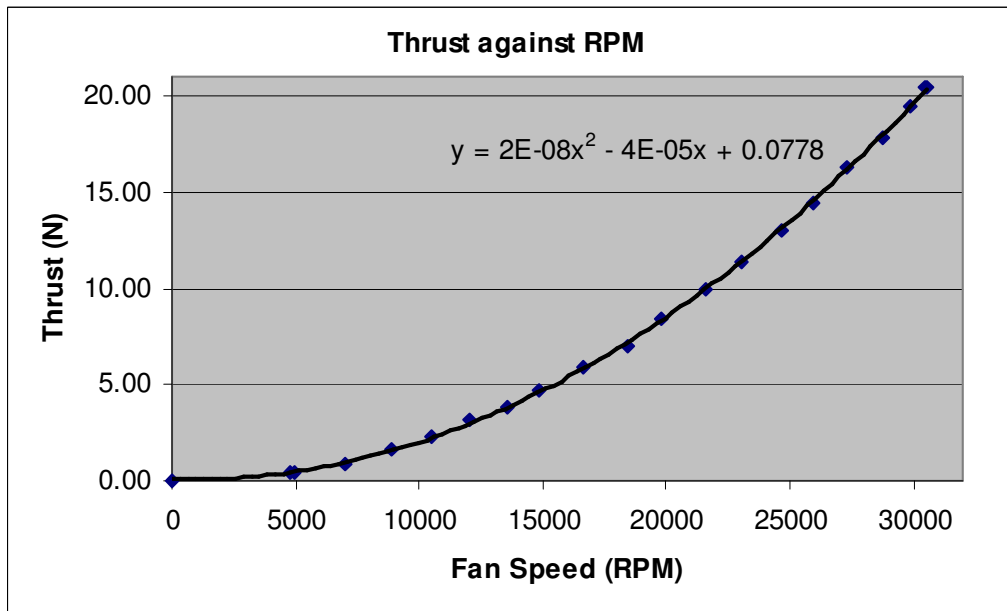


Figure C27: Graph of thrust against fan speed

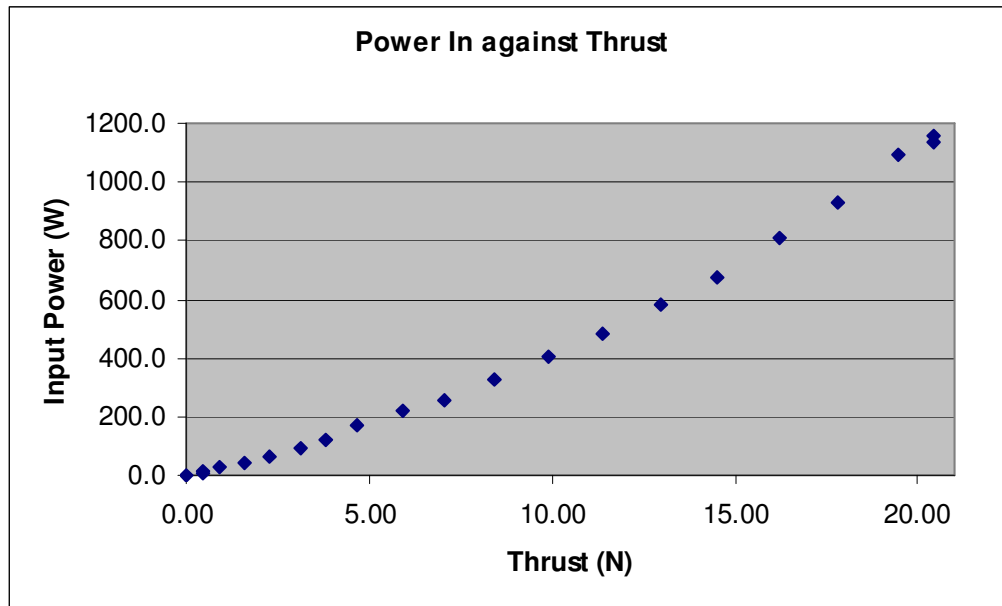


Figure C28: Graph of the input power against thrust

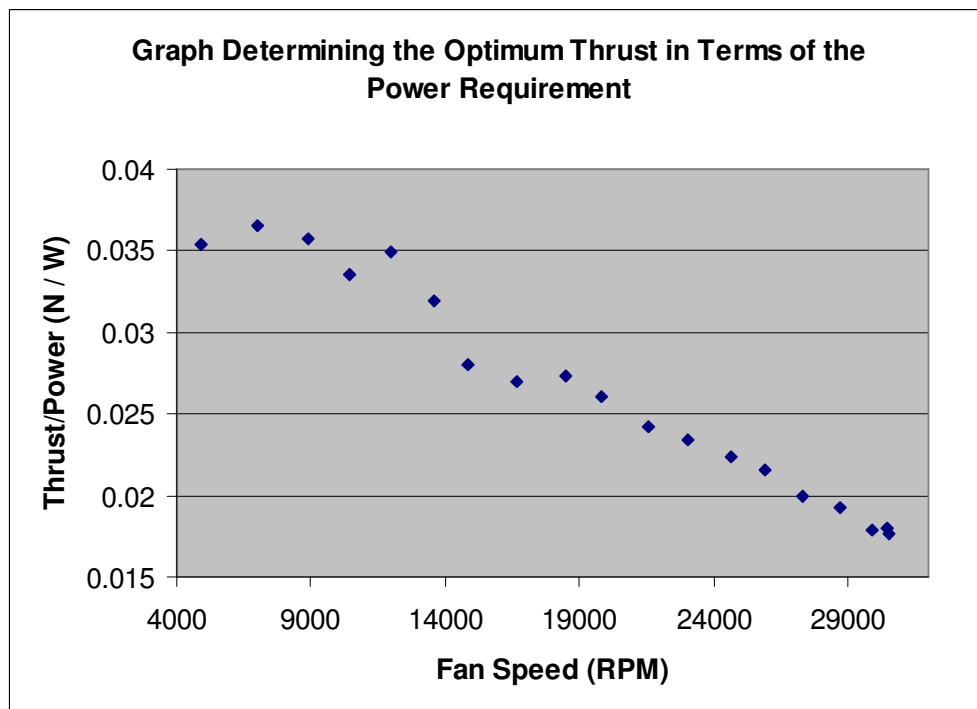


Figure C29: Graph of thrust / power against fan speed

Appendix D

Data and Graphs Produced From Test Results to Experiment 3

Table D11: Shows the response times determined.

% Change	Response Time
60-70	0.25
60-70	0.35
60-70	0.3
mean	0.3
60-50	0.25
60-50	0.3
60-50	0.35
mean	0.3
60-65	0.14
60-65	0.14
60-65	0.14
mean	0.14
60-55	0.1
60-55	0.15
60-55	0.12
mean	0.12

Table D12: Shows the thrust change with time for a 5% step change in pulse width

Time (s)	Thrust (N)
0	14.7
0.02	14.8
0.04	15.1
0.06	15.3
0.08	15.5
0.1	15.65
0.12	15.7
0.14	15.76
0.16	15.8
0.18	15.81
0.2	15.87
0.22	15.92
0.24	15.92
0.26	15.92
0.28	15.92
0.3	15.92

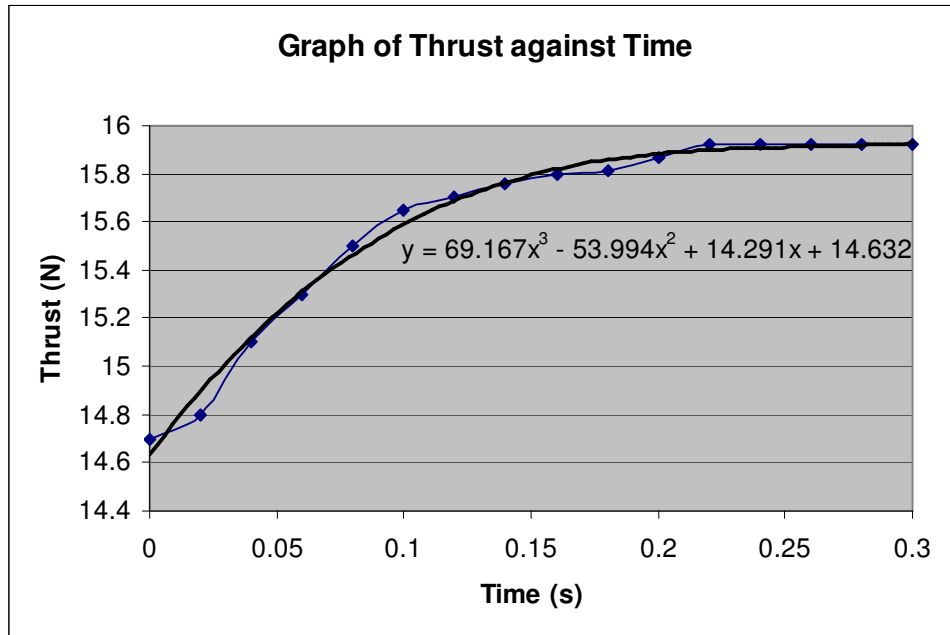


Figure D30: Graph of thrust against time

Appendix E

Data and Graphs Produced From Test Results to Experiment 4

Stage 1: Fans were run at a continuous speed of %60 and the temperature recorded.

Stage 2: Fans were run at an idle speed of %10 to allow an increased rate of cooling.

Stage 3: Fans were switched off and the temperature monitored.

Table E1: Results to stage 1

Time (s)	Temperature (°C)
0	32
20	33
40	36
60	39
80	42
100	44
120	46
140	48
160	50
180	51
200	52
220	53
240	55
260	55
280	56
300	57
320	57
340	58
360	59
380	59
400	59
420	60
440	60
460	61
480	61
500	61
520	62
540	62
560	62
580	63
600	63
620	63
640	63
660	63
680	63
700	63

Table E2: Results to stage 2

Time (s)	Temperature (°C)
0	63
20	75
40	70
60	68
80	65
100	63
120	61
140	59
160	57
180	55
200	54
220	52
240	51
260	50
280	49
300	47
320	47
340	45
360	44
380	43

Table E3: Results to stage 3

Time (s)	Temperature (°C)
0	43
20	46
40	47
60	48
80	48
100	48
120	48
140	48
160	47
180	47
200	47
220	47
240	47
260	46
280	46
300	46

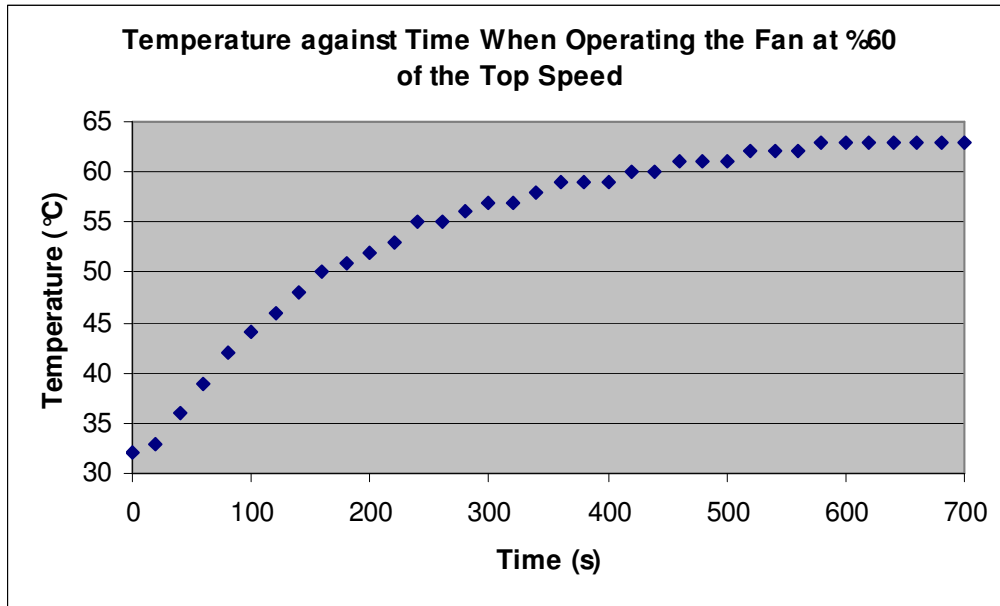


Figure E31: Graph of temperature against time during stage 1

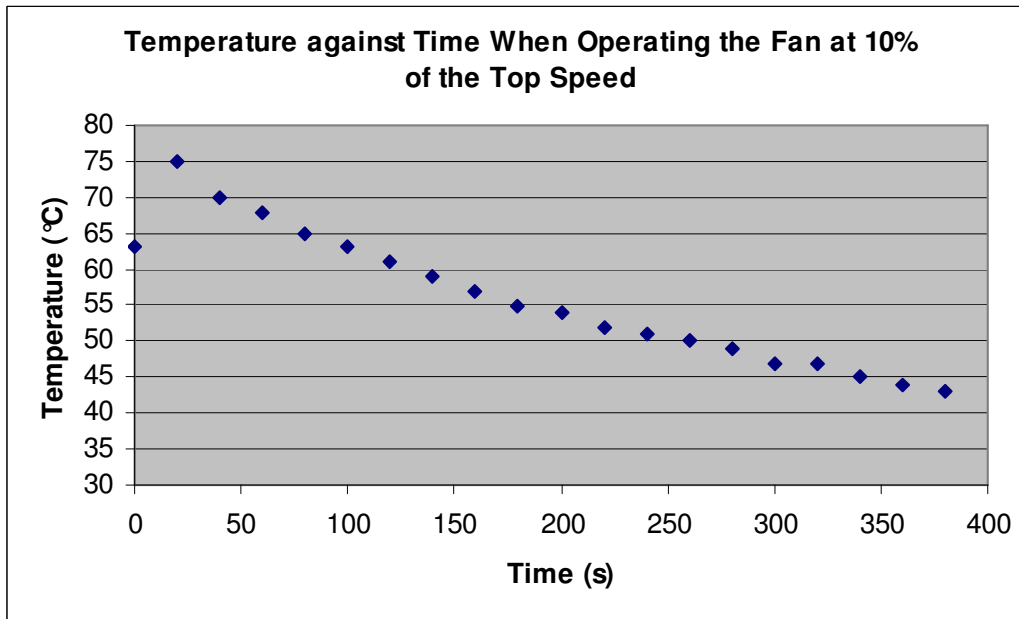


Figure E32: Graph of temperature against time during stage 2

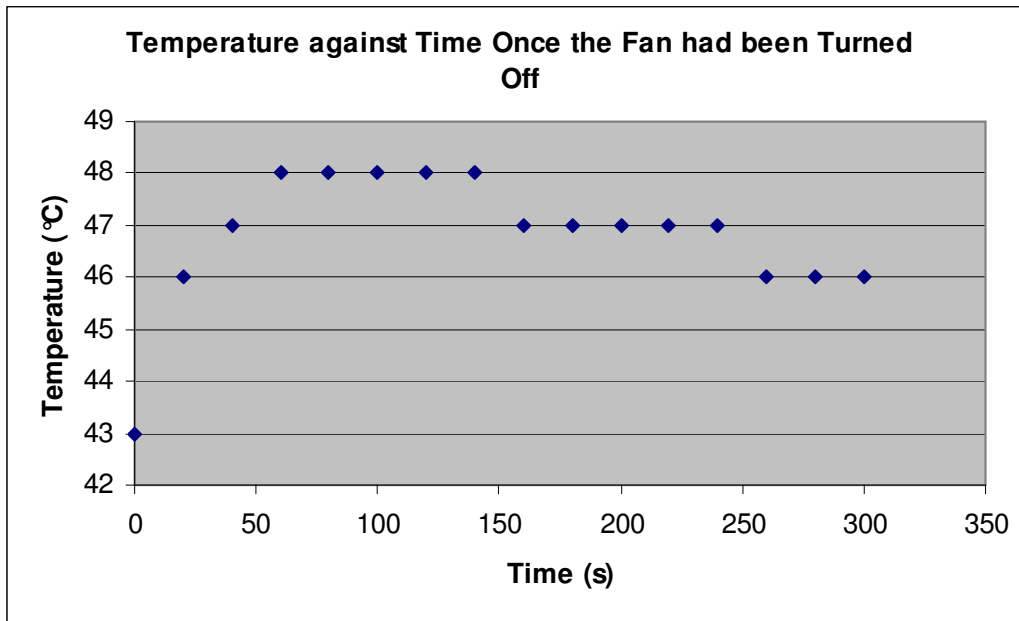


Figure E33: Graph of temperature against time during stage 3

Appendix F

Data and Graphs Produced From Test Results to Experiment 5

Pulse Width (ms)	Voltage Output of Frequency Converter (V)	Frequency (Hz)	Fan Speed RPS	Fan Speed RPM	Mass Reading (g)	Thrust (g)	Thrust (N)
1.00	0.00	0	0.00	0	0	0.00	0.00
1.10	0.74	493	82.22	4933	100	50.50	0.50
1.15	1.05	700	116.67	7000	200	100.99	0.99
1.20	1.33	887	147.78	8867	325	164.11	1.61
1.25	1.57	1047	174.44	10467	470	237.33	2.33
1.30	1.80	1200	200.00	12000	630	318.12	3.12
1.35	2.04	1360	226.67	13600	820	414.06	4.06
1.40	2.23	1487	247.78	14867	1000	504.95	4.95
1.45	2.50	1667	277.78	16667	1245	628.66	6.17
1.50	2.77	1847	307.78	18467	1460	737.23	7.23
1.55	2.97	1980	330.00	19800	1715	865.99	8.50
1.60	3.24	2160	360.00	21600	2000	1009.90	9.91
1.65	3.46	2307	384.44	23067	2280	1151.29	11.29
1.70	3.70	2467	411.11	24667	2600	1312.87	12.88
1.75	3.89	2593	432.22	25933	2940	1484.55	14.56
1.80	4.10	2733	455.56	27333	3280	1656.24	16.25
1.85	4.31	2873	478.89	28733	3620	1827.92	17.93
1.90	4.48	2987	497.78	29867	3960	1999.60	19.62
1.95	4.57	3047	507.78	30467	4165	2103.12	20.63
2.00	4.58	3053	508.89	30533	4175	2108.17	20.68

Table F13: Results to thrust testing at a height of 1.17 m

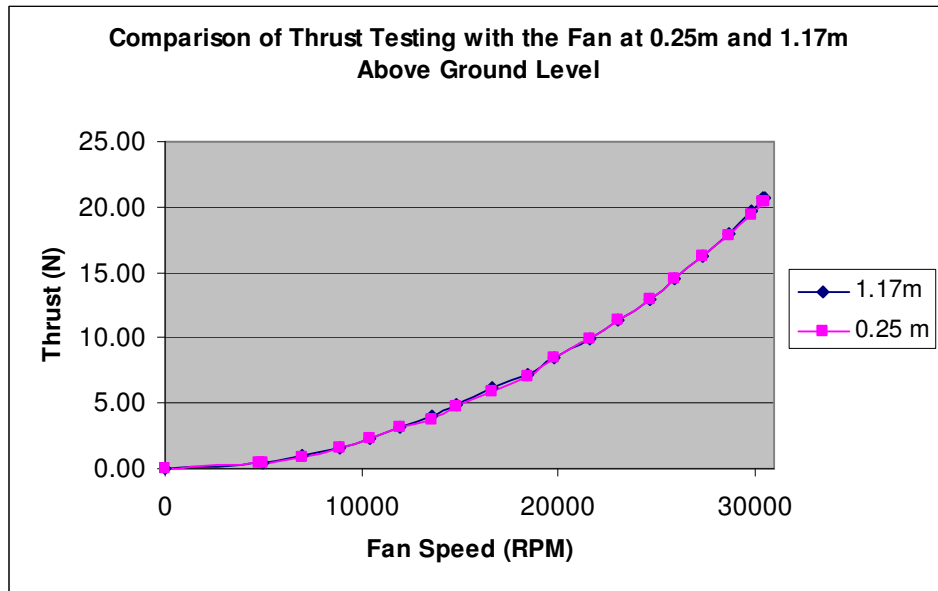


Figure F34: Graph showing thrust test results from experiments 1 & 5

Appendix G

Results from the CFD Analysis

Line 4 (Black) – Represents the velocity magnitude 500 mm downstream of the duct.
 Line 5 (Red) – Represents the velocity magnitude 1000 mm downstream of the duct

N.B. The left side of the duct wall is located at the 0 m position in the graphs with the right side of the duct wall being at 0.13 m position.

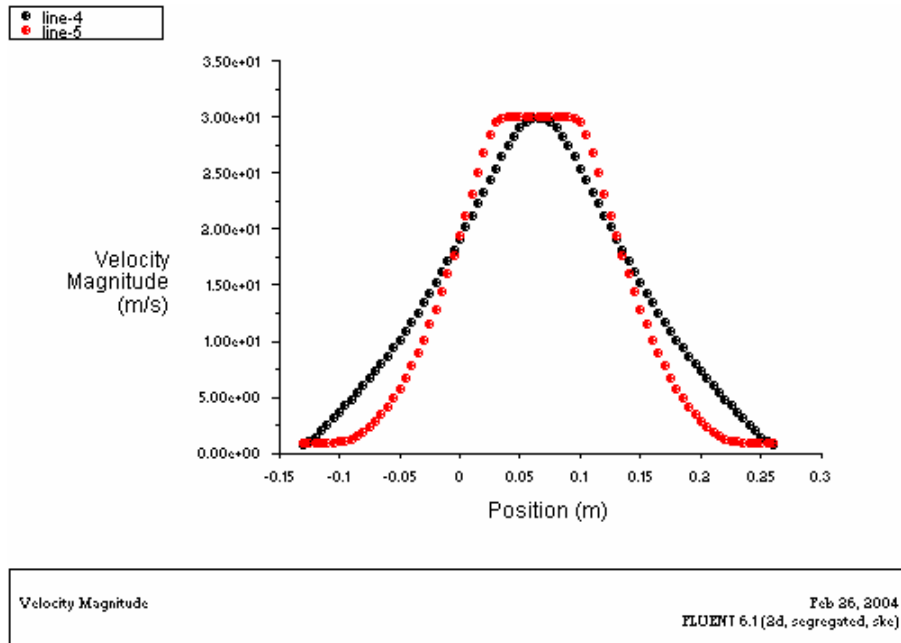


Figure G35: Velocity plot across the stream with an inlet velocity of 30 m/s

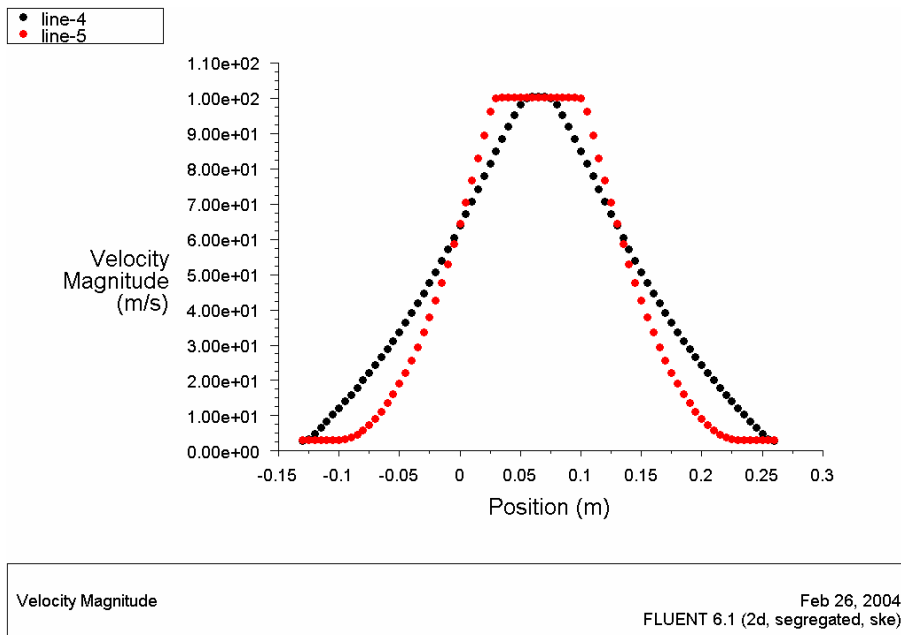


Figure G36: Velocity plot across the stream with an inlet velocity of 100 m/s

Appendix H

Derivation of Equations 19 and 23

Section 1

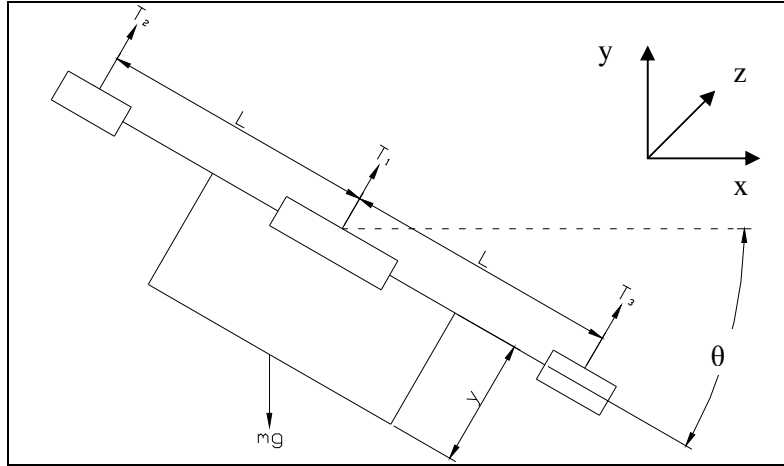


Figure H37: Free Body Diagram of the stability control

Moments produced due to the mass of the platform, M_m , are calculated as follows:

$$M_m = -m \cdot g \cdot y \cdot \sin \theta \quad \text{Equation H78}$$

Moments produce to the thrust of the fans, M_T , are calculated as follows:

$$M_T = T_2 \cdot L - T_3 \cdot L \quad \text{Equation H79}$$

Moments due to the centripetal force produced by the platform precessing, M_C , are calculated as follows:

$$M_C = -m \cdot \omega^2 \cdot y^2 \cdot \sin \theta \cdot \cos \theta \quad \text{Equation H80}$$

Moments produced due to the frictional drag force, M_F , are calculated as follows:

$$M_F = -k_1 \cdot \frac{d\theta}{dt} \quad \text{Equation H81}$$

Moments produced by the drag force, M_D , are calculated as follows:

$$M_D = -k_2 \left(\frac{d\theta}{dt} \right)^2 \quad \text{Equation H82}$$

Summing all these moments to give the total moment acting on this system, results in Equation 19 in the report being produced as follows:

$$M = T_2 \cdot L - T_3 \cdot L - m \cdot g \cdot y \cdot \sin \theta - m \cdot \omega^2 \cdot y^2 \cdot \sin \theta \cdot \cos \theta - k_1 \cdot \frac{d\theta}{dt} - k_2 \left(\frac{d\theta}{dt} \right)^2$$

Section 2

Using the general equation specified in Equation 22 in the report the following non linear terms were linearised as follows:

$$f(\theta) = -m \cdot g \cdot y \cdot \sin \theta \quad \text{Equation H83}$$

$$f(\theta_s + \delta\theta) = m \cdot g \cdot y \cdot \sin \theta_s - m \cdot g \cdot y \cdot \cos \theta_s \cdot \delta\theta \quad \text{Equation H84}$$

$$\therefore f(\theta_s + \delta\theta) = -m \cdot g \cdot y \theta \quad \text{Equation H85}$$

$$f(\theta) = -m \cdot \omega^2 \cdot y^2 \cdot \sin \theta \cdot \cos \theta \quad \text{Equation H86}$$

$$f(\theta_s + \delta\theta) = -m \cdot \omega^2 \cdot y^2 \cdot \sin \theta_s \cdot \cos \theta_s - m \cdot \omega^2 \cdot y^2 \cdot \cos \theta_s \cdot \cos \theta_s \cdot \delta\theta + m \cdot \omega^2 \cdot y^2 \cdot \sin \theta_s \cdot \sin \theta_s \cdot \delta\theta$$

- Equation H87

$$\therefore f(\theta_s + \delta\theta) = -m \cdot \omega \cdot y^2 \cdot \theta \quad \text{Equation H88}$$

$$f(\theta) = -k_2 \left(\frac{d\theta}{dt} \right)^2 \quad \text{Equation H89}$$

$$f(\theta_s + \delta\theta) = 0 \quad \text{Equation H90}$$

Equations H8, H11, and H13 can now replace their non linear equivalents to form Equation 23 in the report.

Appendix I

Table of Laplace Transform Pairs

*Not included in the CD copy of this report.
This information is freely available in text books.*

Appendix J

Formation of a Routh Array

Assuming a characteristic equation to be expressed in general terms by Equation II below, the following corresponding Routh array can be constructed.

$$q(s) = s^6 + a_5 \cdot s^5 + a_4 \cdot s^4 + a_3 \cdot s^3 + a_2 \cdot s^2 + a_1 \cdot s + a_0 \quad \text{Equation I91}$$

$$\begin{array}{l|llll} s^6 & 1 & a_4 & a_2 & a_0 \\ s^5 & a_5 & a_3 & a_1 & 0 \\ s^4 & b_4 & b_2 & b_0 & 0 \\ s^3 & c_3 & c_1 & 0 & 0 \\ s^2 & d_2 & d_0 & 0 & 0 \\ s & e_1 & 0 & 0 & 0 \\ s^0 & f_0 & 0 & 0 & 0 \end{array}$$

The constants in the Routh array can then be determined as follows:

$$b_4 = \frac{-1}{a_5} \begin{vmatrix} 1 & a_4 \\ a_5 & a_3 \end{vmatrix} \quad b_2 = \frac{-1}{a_5} \begin{vmatrix} 1 & a_2 \\ a_5 & a_1 \end{vmatrix} \quad b_0 = \frac{-1}{a_5} \begin{vmatrix} 1 & a_0 \\ a_5 & 0 \end{vmatrix}$$

$$c_3 = \frac{-1}{b_4} \begin{vmatrix} a_5 & a_3 \\ b_4 & b_2 \end{vmatrix} \quad c_1 = \frac{-1}{b_4} \begin{vmatrix} a_5 & a_1 \\ b_4 & b_0 \end{vmatrix}$$

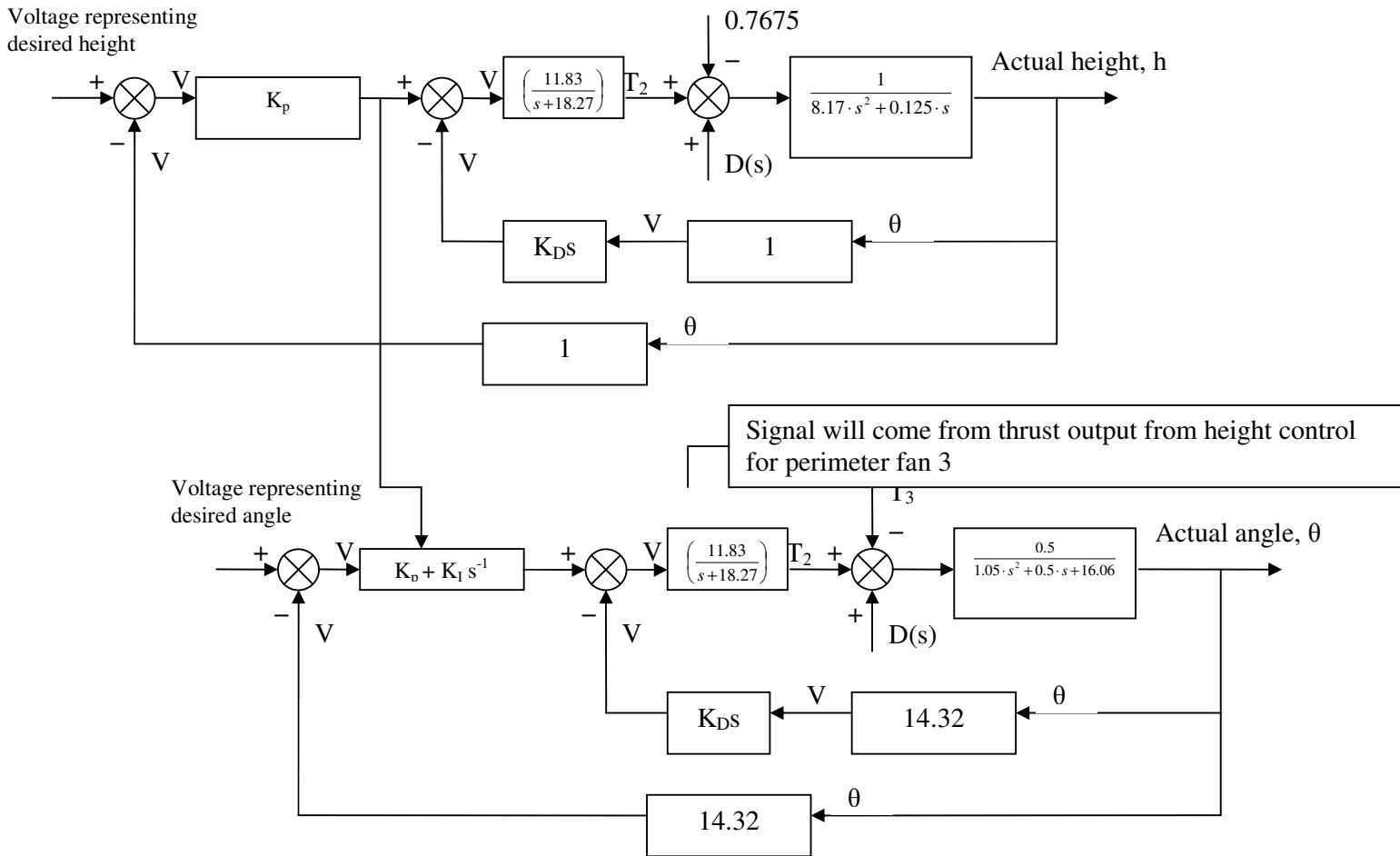
$$d_2 = \frac{-1}{c_3} \begin{vmatrix} b_4 & b_2 \\ c_3 & c_1 \end{vmatrix} \quad d_0 = \frac{-1}{c_3} \begin{vmatrix} b_4 & b_0 \\ c_3 & 0 \end{vmatrix}$$

$$e_1 = \frac{-1}{d_2} \begin{vmatrix} c_3 & c_1 \\ d_2 & d_0 \end{vmatrix}$$

$$f_0 = \frac{-1}{e_1} \begin{vmatrix} d_2 & d_0 \\ e_1 & 0 \end{vmatrix}$$

Appendix K

Combined Block Diagram of the Height and Stability Control



8. References

- [1] Group project report, (2003), *The Design and Development of a Flying Platform*, School of Engineering, University of Exeter.
- [2] Moore, Stephen, (2003), *The Design and Development of a Flying Platform*, Individual Report, School of Engineering, University of Exeter.
- [3] Motor specification sheet, *Plettenberg HP220/30/A4 S P4 SL*
- [4] Tombling, Alex, (2004), *The Design and Development of a Flying Platform*, Individual Report, School of Engineering, University of Exeter.
- [5] Poczka, Christopher, (2004), *The Design and Development of a Flying Platform*, Individual Report, School of Engineering, University of Exeter.
- [6] S. Moores Report (2003), *The Design and Development of a Flying Platform*, Individual Report, School of Engineering, University of Exeter.
- [7] Forder, Richard, (2004), *The Design and Development of a Flying Platform*, Individual Report, School of Engineering, University of Exeter.
- [8] Holbrook, Richard, (2004), *The Design and Development of a Flying Platform*, Individual Report, School of Engineering, University of Exeter.
- [9] Bishop, Robert, (1997), *Modern Control Systems Analysis and Design*, The University of Texas at Austin.